

# Transition from slab roll-back to slab break-off in the central Apennines, Italy: Constraints from the stratigraphic and thermochronologic record

Maria Giuditta Fellin<sup>1,†</sup>, Malwina San Jose<sup>1,2</sup>, Claudio Faccenna<sup>2,3</sup>, Sean D. Willett<sup>1</sup>, Domenico Cosentino<sup>2</sup>, Riccardo Lanari<sup>2,4</sup>, Loraine Gourbet<sup>1</sup>, and Colin Maden<sup>1</sup>

<sup>1</sup>Department of Earth Sciences, ETH Zürich, Sonneggstrasse 5, 8092 Zurich, Switzerland

<sup>2</sup>Dipartimento di Scienze, Università degli Studi Roma Tre, Largo S.L. Murialdo, 1, 00146 Roma, Italy

<sup>3</sup>Jackson School of Geosciences, University of Texas at Austin, Austin, Texas, USA

<sup>4</sup>Dipartimento di Scienze della Terra, Università degli Studi di Firenze, Via La Pira 4, 50121 Firenze, Italy

## ABSTRACT

Stratigraphic and thermochronologic data are used to study the processes that shaped the topography of the central Apennines of Italy. These are part of a major, active mountain belt in the center of the Mediterranean area, where several subduction zones control a complex topography. The Apennines were shaped by contraction at the front of the accretionary wedge overlying the subducting Adria microplate followed by extension at the wedge rear in response to eastward slab roll-back. In the central Apennines, intermontane extensional basins on the western flank rise eastward toward the summit. We contribute with new data consisting of 28 (U-Th-Sm)/He and 10 fission track ages on apatites to resolve a complex pattern of thermal histories in time and space, which we interpret as reflecting the transitional state of the orogen, undergoing a two-phase evolution related to initial slab retreat, followed by slab detachment. Along the Tyrrhenian coast, we document cooling from depths  $\geq 3$ –4 km occurring between 8 and 5 Ma and related to the opening of marine extensional basins. Post-5 Ma, a broader region of the central Apennines exhibits cooling from variable depths, between  $< 2$  km in most areas and  $\geq 3$ –4 km in the northeast, and with different onset times: at ca. 4 Ma in the west, at ca. 2.5 Ma in the center and northeast, and at ca. 1 Ma in the southeast. Between 5 and 2.5 Ma, exhumation is associated with modest topographic growth during the late stages of thrusting. Since 2.5 Ma, exhumation has concurred with the opening of intermontane basins in

the west and in the east, with regional topographic growth and erosion, that we interpret to be associated with the locally detaching slab.

## 1. INTRODUCTION

The elevated surface topography of mountain belts impacts the local and global climate and hosts biodiversity hotspots. Important clues to the dynamics of these systems could come from the study of the surface evolution of orogens. Yet, the erosive nature of mountainous landscapes makes it challenging to find markers of the uplift process of an orogen. Here we study the case of the central Apennines of Italy, one of the most elevated topographic barriers in the Mediterranean area, where surface topography is controlled tectonically by an intricate system of multiple subduction zones.

The Apennine Mountains of Italy are an active orogenic belt overlying the subducting Adria microplate (Fig. 1). The highest ranges of the Apennines are in their central region, where the western flank, dissected by active normal faults (e.g., Pondrelli et al., 2006), rises gently from the backarc basin for over a 100 km reaching up to  $\sim 3000$  m above sea level (a.s.l.) whereas the eastern flank slopes toward the submerged foreland over less than 50 km. For a long time, from the late Oligocene to the late Miocene, while the Adriatic slab retreated eastward for hundreds of kilometers, on the western side of the Apennines normal faulting typically overprinted compressive structures, depressed and subsided the surface topography toward the back-arc rift, i.e., the Tyrrhenian Basin, resulting in limited denudation (Malinverno and Ryan, 1986; Royden et al., 1987; Royden, 1993; Royden and Faccenna, 2018). Since the Pliocene, surface topography above sea level and denudation have become significant (e.g., Fellin et al., 2007; Thomson),

and extensional deformation has extended on land with the formation of intermontane basins (e.g., Patacca et al., 1990; Boccaletti et al., 1990; Cipollari and Cosentino, 1995a, 1995b; Cosentino et al., 2010). This pulse of surface uplift above sea level at the same time with the formation of extensional intermontane basins has been interpreted as indicative of a change in the orogenic dynamics. The various mechanism called upon to explain the recent uplift above sea level all postulate a change in the subduction dynamic as for instance: slab break-off (Wortel and Spakman, 2000; Gvirtzman and Nur, 2001; Faccenna et al., 2014; Faure Walker et al., 2012), mantle upwelling (D'Agostino et al., 2001), or crustal delamination (Cavinato and DeCelles, 1999). As for slab-roll back, the underlying commonality among these different processes is the influence of subduction and the related mantle dynamics on the upper plate. Subduction can affect upper plate topography in a variety of ways: the pull exerted by the subducting slab and the induced return flow can depress the forearc regions by some hundreds of meters (Zhong and Gurnis, 1994), whereas the upwelling associated with return flow or small-scale convection can induce a positive signal in the backarc regions (Zhong and Gurnis, 1994; Hyndman and Currie, 2011; Crameri et al., 2017; Faccenna and Becker, 2020). This scenario can change with a decrease in subduction pull and subduction rate as in, for example, the case of slab break-off (e.g., Duretz and Gerya, 2013). However, other processes can control the upper plate topography as, for instance, the accretion of crustal material from the down-going plate that can counter the upper plate subsidence. In particular, if continental crustal material is brought into the subduction zone, detached from the lithosphere and accreted into the upper plate crust, its buoyancy can lead to surface uplift (Göğüş et al., 2017). Thus, the spatial and temporal patterns of uplift in a

Maria Giuditta Fellin  <https://orcid.org/0000-0003-3545-3512>

<sup>†</sup>giuditta.fellin@erdw.ethz.ch.

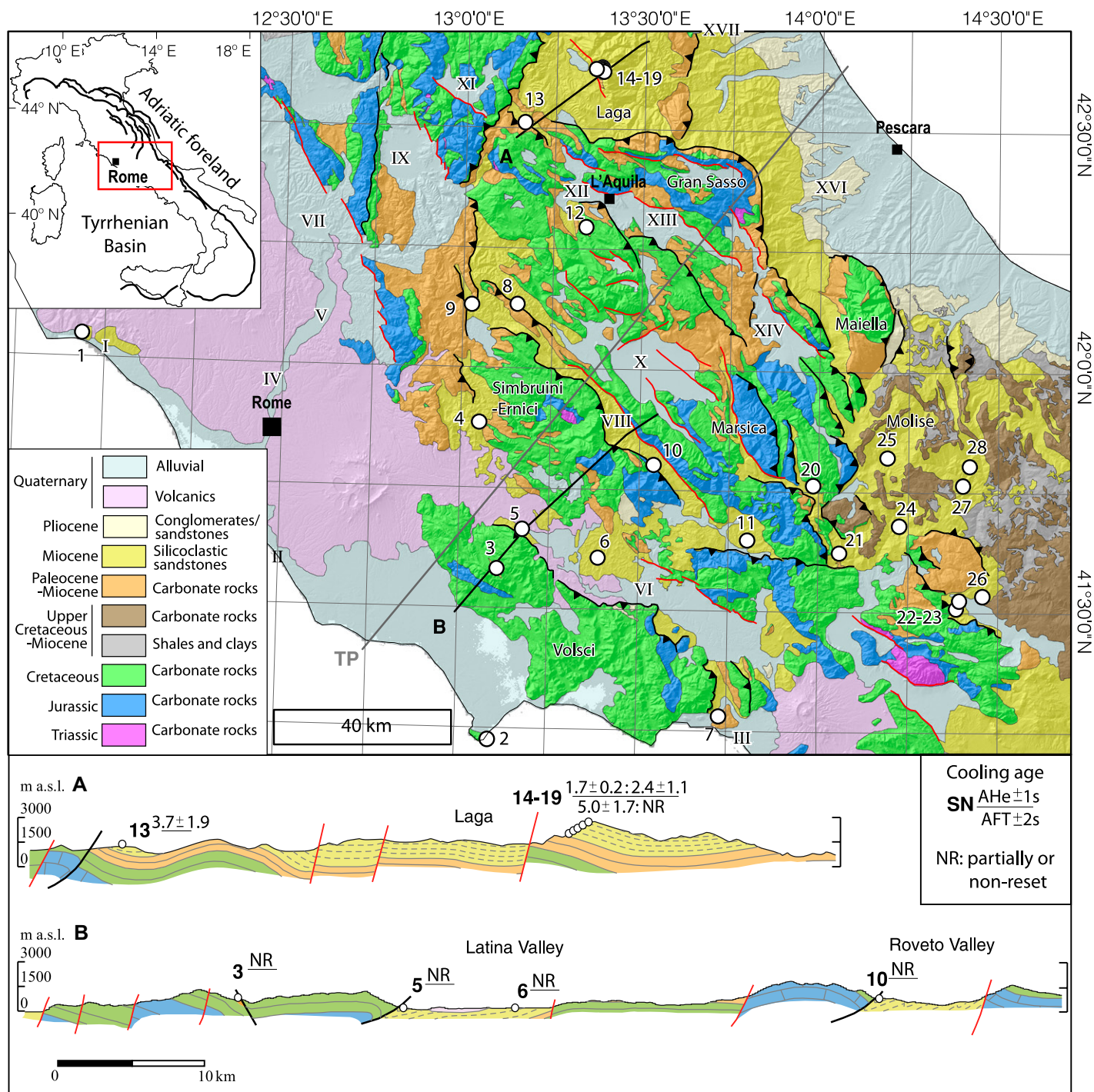


**Figure 1.** Inset: map of Italy. Thick black lines indicate the surface and subsurface main thrusts of the Apennines. Red box in center outlines the location of the geologic map in the main panel. Main panel: simplified geologic map of the central Apennines with sample locations indicated by Arabic numerals from 1 to 28. A and B indicate the traces of the geologic cross-sections shown in the lower panel. TP is the trace of topographic swath profile and of the sample projection shown in Figure 5. Roman numerals indicate the location of coastal and interapenninic basins, whose stratigraphic record is schematically shown in Figure 2. Topographic names refer to main mountain ranges or regions that correspond to structural-kinematic units whose stratigraphic record is also schematically shown in Figure 2. Lower panel: simplified geologic sections across the central Apennines with projected cooling ages: the location of the sections is indicated in the main panel. The vertical and horizontal scales are the same. m.a.s.l.—meters above sea level; AFT—apatite fission-track; AHe—(U-Th-Sm)/He ages; SN—sample number.

subduction forearc can be complex due to the interaction of these processes.

In the central Apennines, origin and mechanism of surface uplift remain unclear: did the central Apennines started to emerge when crustal thickening outpaced the depression induced by the slab pull? Or did they emerge in the extensional “back-arc” due to the positive signal induced by mantle upwelling? Or are they a late-orogenic transient, related to slab break-off? The transition in time and space between end of contraction, surface uplift above sea level, and onset of on-land extension are keys to address these questions. So far, it has been proposed that between the late Miocene and the present, surface uplift may have migrated eastward following contraction and extension (e.g., Cavinato and DeCelles, 1999), or that it may have resulted from a regional doming with only minor local uplift related to extension and/or contraction (e.g., D’Agostino et al., 2001). Recent paleo-elevation data based on stable isotopes indicate 1–2 km of surface uplift initiating in the late Pliocene (San Jose et al., 2020) and stratigraphic data suggest that both in the western and in the eastern intermontane basins of the central Apennines deposition may have started at the same time, during the late Pliocene (Cosentino et al., 2009, 2017).

In this study, we combine new thermochronology data and a revised stratigraphic assessment of syn-tectonic basins in the central Apennines to track the vertical crustal motions during the late stage of subduction orogeny. Low-temperature thermochronology is sensitive to surface and crustal processes at shallow depths and tracks the rocks toward the surface along their exhumation path. In particular, it is very effective at detecting rapid cooling related to the activity of normal faults and therefore it can provide new constraints on the timing of the extensional activity. We use the stratigraphic record to time the transition from marine to terrestrial conditions that generally corresponds to the transition from a non-erosive to erosive condition. The timing of this transition can correspond to the onset of cooling if exhumation is driven by erosive surface processes. Based on the tectono-stratigraphic record, it is also possible to reconstruct when—within the sedimentary basins—contractional or extensional deformation was active. Our data support the idea that a change in subduction dynamics, from trench retreat to slab break-off occurred in this area around the early Pleistocene, perturbing the topography, tectonics, and sedimentation pattern of the orogen.

## 2. GEOLOGICAL BACKGROUND

The Apennines of Italy originated as a Neogene fold-and-thrust belt during the west-verging

subduction of the Adria micro-plate (Malinverno and Ryan, 1986; Royden et al., 1987; Patacca et al., 1990; Royden and Faccenna, 2018). The roll back of the Adria-Ionian subduction system resulted in progressive north-eastward migration of the foreland basin system, extension at the back of the growing wedge and backarc rifting that led to the opening of the Tyrrhenian Basin since the late Serravallian (Mattei et al., 2002). Subduction of Adria in the central Apennines involved the accretion of a sequence of Jurassic to Miocene limestones, deposited as carbonate shelf platforms and/or slope-to-basin sediments along the Adria passive margin (e.g., Cosentino et al., 2010). With the passive margin entering the foreland, the platforms drowned and became the bedrock for clastic turbiditic sediments that until the late Miocene were fed predominantly from the Alps (e.g., Stalder et al., 2018 and references therein). As the wedge migrated north-east, the foreland system evolved into thrust-top basins and then it was rapidly incorporated into the wedge (Boccaletti et al., 1990; Cipollari and Cosentino, 1992, 1995a; Fig. 2). With crustal shortening moving toward more external domains, the Tyrrhenian Basin expanded eastward and extensional faults dissected the emerging inner portion of the accretionary wedge. These faults are seismically active (Pondrelli et al., 2006; Chiarabba et al., 2005) and bound intermontane basins and front-parallel valleys that accumulated terrestrial and marine sediments since at least the latest Pliocene (Cavinato et al., 1994; Cavinato and DeCelles, 1999; Cosentino et al., 2017; Figs. 1 and 2). Based on unconformably overlying sediments in the Adriatic foredeep (Casero, 2004), compression in the central Apennines may have ceased in the late Pliocene (Bigi et al., 2013). During the Pliocene–Pleistocene, igneous activity developed along the Tyrrhenian side of the central Apennines (Conticelli and Peccerillo, 1992), where a high heat flux ( $>100 \text{ mW m}^{-2}$ ; Cataldi et al., 1995) persists today over a shallow and anomalously hot Moho (Diaferia et al., 2019) and over a low velocity anomaly in the upper mantle (Wortel and Spakman, 2000; Piromallo and Morelli, 2003). The central and Adriatic sides of the central Apennines are characterized by a colder thermal regime (heat flux  $<50 \text{ mW m}^{-2}$ ) at shallow crustal levels and by a deep hot thermal regime ( $>300 \text{ mW m}^{-2}$ ; Chiodini et al., 2013).

## 2.2. Compression and Extension in the Central Apennines

The marine successions of the Apennine foreland basin system and the marine-to-continental successions of the intermontane basins provide

constraints on the chronology of vertical motions in the Apennines. Syn-tectonic basins are associated with both contractional and extensional deformation, forming as foredeeps, wedge-top basins or extensional grabens and tilt-block half-grabens. Along a stratigraphic section, the transition of the depositional environment from marine foredeep to wedge-top basin and finally to terrestrial extensional basin provides constraints on the surface vertical motion, with high resolution in space and time. The most unambiguous constraint is provided by the transition from marine to terrestrial facies, which marks passage through sea level. We have compiled stratigraphic data from the central Apennines and constructed 22 stratigraphic sections whose location and sedimentary successions are shown in Figures 1 and 2, respectively, where they are indicated with roman numbers.

### 2.2.1. Foreland Successions

In the western sector of the study area, along the Tyrrhenian coast, limited rock exposures of foredeep siliciclastic sandstones attributed to the Aquitanian are in the south (near sample 2, Fig. 1; CGI Terracina, 1960). These sandstones in cores along the Tyrrhenian coast are overlain by Neogene deposits, mainly consisting of upper Messinian gypsum deposits and Lago-Mare conglomerates and sandstones deposited in extensional basins. Plio-Pleistocene clays and sands are locally interlayered with Pleistocene volcanic rocks (e.g., I: Tolfa, De Rita et al., 1997; Cipollari et al., 1999b; II: Ardea and Formia basins, Faccenna et al., 1994; III: Garigliano Basin, Cosentino et al., 2006). Inland, the Mesozoic–Miocene carbonate rocks in the Volsci and Simbruini-Ernici ranges are thrust over the Latina and Roveto valleys (VI and VIII), respectively, that are filled with foredeep siliciclastic sediments. Autochthonous Serravallian marls mark the flexure of the foreland domain in the Volsci range that likely was already in a wedge-top position during the late Tortonian (Cosentino et al., 2003). The Latina valley (VI) was a foredeep basin that received up to 2 km of upper Tortonian sands (Frosinone unit) and locally preserves unconformable lower Messinian sandstones related to an early Messinian thrust-top basin (e.g., Torrice Sandstones, Cipollari and Cosentino, 1993, 1995a, 1995b; Cosentino et al., 2002, 2003; Centamore and Rossi, 2009). In the Simbruini-Ernici range and the Roveto valley (VIII), onset and end of deposition in the central Apennine foreland basin system are timed by upper Tortonian foreland marls, lower Messinian siliciclastic foredeep sandstones and two cycles of wedge-top sediments, extending to the uppermost Messinian–lower Zanclean (Cosentino et al., 2003).

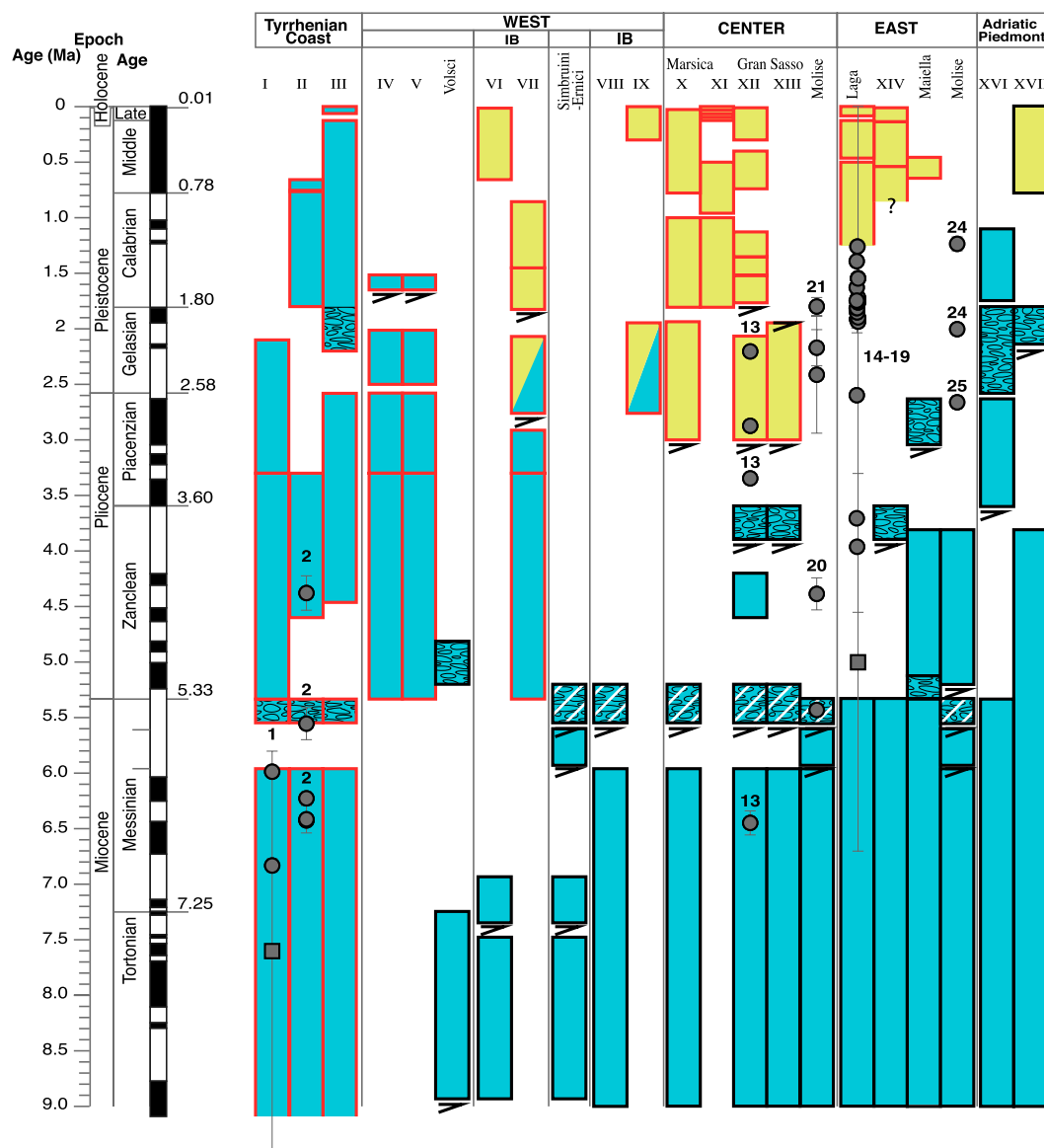
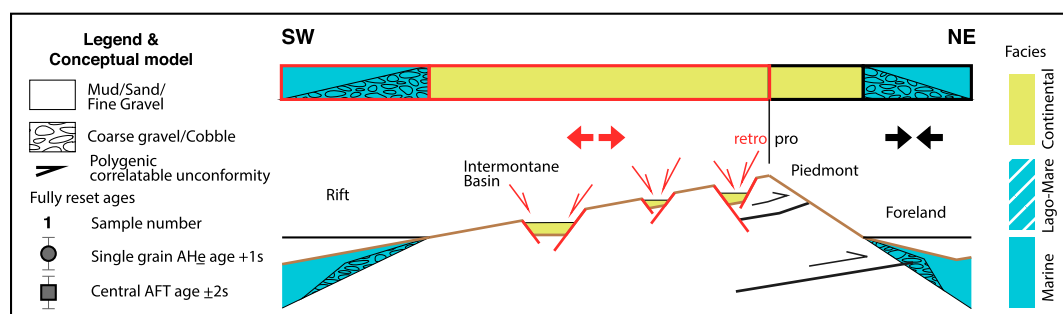


Figure 2. Comparison between fully reset cooling ages from this study and the foreland and intermontane stratigraphic record from previous studies in the central Apennines, Italy. The stratigraphic record is shown as a west-to-east and north-to-south schematic summary of the stratigraphic successions in the main ranges and basins of the central Apennines; references are reported in the main text (section 2). Arabic numerals refer to the coastal and intermontane basins whose locations are shown in Figure 1. The foreland successions exposed in the Molise region are split in two columns: one labeled Centre that shows older, internal units and one labeled East that shows younger, more external units. No intermontane basin is present in Molise. The inset above the figure shows the legend together with a conceptual scheme that represents the main features of the Apenninic orogenic wedge since the Pliocene, which are: the Tyrrhenian rift basin on the west, the intermontane extensional basins on the top, the piedmont slope and the foreland basin on the east. The foreland basin system successions consist of marine (blue) terrigenous sediments deposited in different basins and settings (ramp, foredeep and wedge-top) within the east-ward migrating and contractionally (black outline) deforming foreland system. The only non-marine terrigenous foreland sediments are exposed at present along the Adriatic piedmont. The foreland sediments overlie marine carbonate sediments that are not indicated in the figure. No marine carbonate sediments lie

over or alternate with the foreland sediments. The intermontane successions consist of marine, transitional and continental (yellow) sediments filling intermontane extensional (red outline) basins that develop on the retro side of the orogenic wedge as the compressional front migrates eastward. The white diagonal lines over the blue symbol refer to Lago-Mare deposits. The position of the apatite (U-Th-Sm)/He (AHe) grain ages and central apatite fission-track (AFT) ages corresponds to the closest structural unit.



In the central sector of the study area, the Gran Sasso and Maiella massifs represent the highest and easternmost ranges of the Apennines. Limited foredeep sediment outcrops are commonly lower Messinian in age (X to XIII: Patacca et al., 1992; Cipollari and Cosentino, 1995b) but in the east they extend in age to the top of the Messinian (XIV: Patacca et al., 1992; Cipollari and Cosentino, 1995b; Centamore et al., 2006c). Two cycles of terrigenous Lago-Mare and marine conglomeratic wedges (wedge-top basins) record thrusting activity until the latest Zanclean–earliest Piacenzian (Cipollari et al., 1999a; Cosentino et al., 2003; Centamore et al., 2006a and references therein). In the Maiella, an outmost anticlinal tectonic structure (Vezzani et al., 2010 and references therein), Messinian foreland mudstones and marly clays are covered by Zanclean conglomerates and turbidites (Maiella and Cellino units) and finally by Piacenzian thrust-top clastic deposits (Patacca et al., 1992, 2008; Cipollari et al., 1999b; Cosentino et al., 2005).

The central massifs slope toward the Laga Mountains to the north, the Adriatic piedmont to the east and the Molise hills to the south. The Laga Mountains consist of a ~4-km-thick succession of Messinian turbiditic siliciclastic sandstones that filled a foredeep sub-basin where drowning started at the transition between middle and upper Tortonian (Centamore et al., 1992; Cosentino et al., 2003) and where syn-deposition contraction occurred since the late Messinian, leading to eastward migration of the foredeep during the Zanclean (Bigi et al., 2011). Along the Adriatic Piedmont, north of the study area, Piacenzian–Gelasian marine clastic wedges, overlying Messinian–lower Zanclean foredeep sandstones and in turn overlain by shallowing-upward, marine-to-continental transitional successions, are bound at the top by a polygenic erosional unconformity (Cantalamezza and Di Celma, 2004; Micarelli and Cantalamezza, 2009) that has also been traced farther south in our study area. There, steeply dipping upper Messinian–lower Zanclean foredeep sandstones are overlain by Gelasian flat-lying marine littoral conglomerates (Pizzi, 2003) that pass to lower-middle Pleistocene continental sediments. In the Molise Hills (Fig. 1), low-competence, non-carbonate rocks are part of a far traveled complex (Sicilide unit), largely consisting of Cretaceous-to-middle Miocene shales and clays, which first thrust over 2-km-thick, upper Tortonian (?)–lower Messinian siliciclastic turbidites (Agnone Formation) and their substratum (Molise units), later over Zanclean clayish deposits (Torrente Lajo Flysch) and finally was in turn covered unconformably covered by sediments from late Messinian–Zanclean thrust-top basins (Festa

et al., 2006; Vezzani et al., 2010; Cosentino et al., 2018).

## 2.2.2. Intermontane Successions

In the Pliocene-to-Holocene extensional intermontane basins, the base of the non-marine succession provides a minimum age for the onset of extension but in several basins the base is either not exposed (e.g., X: Fucino Basin, Cavinato et al., 1994) or erosive with a large time gap following the foreland basin system succession (e.g., VII: Tiberino Basin, Mancini et al., 2007; Cosentino et al., 2017). The western intermontane basins, north of Rome (VII and IX: Tiberino and Rieti basins; Figs. 1 and 2), were filled with uppermost Piacenzian–Gelasian, lacustrine continental fluvial sediments, laid with an angular unconformity over the Mesozoic–Cenozoic bedrock (Mancini et al., 2007; Fubelli et al., 2014; Cosentino et al., 2008, 2017). Upper Piacenzian–Gelasian to Gelasian sediments are also the basal lacustrine and fluvial infill of the central intermontane basins (X: Fucino; Cavinato et al., 2002; Centamore et al., 2006b; Giaccio et al., 2019; Mondati et al., 2021; XI and XII: L'Aquila; Cosentino et al., 2017). In the other eastern intermontane basins (XI, Leonessa Basin; XII: Sulmona Basin; Amatrice Basin in the Laga Mountains), the stratigraphic record does not go back in time beyond the Calabrian (Cavinato et al., 1994; Fubelli et al., 2008; Giaccio et al., 2013; Mancini et al., 2020).

The onset of the infill of the intermontane basins was followed toward the end of the Gelasian by a regional scale event that can be traced across the central Apennines. Along the Tyrrhenian coast, a non-depositional hiatus during the Gelasian marked by an angular unconformity and locally thick conglomerates is recorded within the marine successions at several locations (Cosentino et al., 2006). This unconformity has been correlated to: a large angular unconformity and hiatus at two sites near Rome (IV and V: Monte Mario and Vallericca; Figs. 1 and 2) below Calabrian marine littoral sediments and above marine bathyal sediments that are Zanclean and lower Gelasian in age, respectively (Cosentino et al., 2009); an angular erosional unconformity overlain by Calabrian-to-Holocene fluvial-lacustrine successions in the Tiberino Basin (VII); an abandonment surface in the Rieti Basin (IX) and two erosional and abandonment surfaces within the L'Aquila Basin (XIII: Cosentino et al., 2017). An erosional unconformity in a central intermontane basin (X: Fucino) separates the Gelasian lacustrine lower unit from the Calabrian to Holocene upper unit (Cavinato et al., 2002; Centamore et al., 2006b; Giaccio et al., 2019; Mondati et al., 2021). A late Gelasian polygenic erosional surface, described

in section 2.2.1, is also traceable along the Adriatic Piedmont.

## 3. METHODS

### 3.1. Sample Strategy and Analytical Technique

The siliciclastic sediments filling the foreland basin systems of the central Apennines were the target of our sampling for apatite fission-track (AFT) and (U-Th-Sm)/He (AHe) dating of apatites as these deposits are the only apatite-bearing rocks exposed in the central Apennines, due to their Alpine provenance (Stalder et al., 2018). We used vitrinite reflectance (Ro) data from previous studies (Table 1; Corrado, 1995; Corrado et al., 1998, 2005; Rusciadelli et al., 2005; Aldega et al., 2007) to identify potential thermochronologic sampling sites where maximum burial conditions should have exceeded 40 °C, indicated by a Ro  $\geq 0.30\%$  as these sites could provide thermochronologically reset samples. In cases where no vitrinite data is available, we sampled the lowermost outcropping unit in the sedimentary sequence to maximize burial depth, as well as the closest locations to thrust faults where the samples might have been subjected to tectonic burial prior to exhumation (Fig. 1). Moreover, we constructed one age-elevation profile by collecting six samples from the foot-wall of a large extensional fault (Monte Gorzano fault, Fig. 1), between 1572 m and 2154 m a.s.l., and one sample from its hanging wall.

Coordinates, structural position, depositional age, and constraints on burial conditions for all samples are summarized in Table 1, where we report the sample name together with the sample number (N) that is used in all the figures. Based on their depositional age and structural position, from SW (Tyrrhenian) to NE (Adriatic), our samples can be divided in five groups (Fig. 3) that include: pre-Tortonian samples along the Tyrrhenian coast (samples 1 and 2) and in the Volsci range (sample 3); upper Tortonian samples in the Latina valley (samples 4–7) and lower Messinian samples in the Roveto valley (samples 8–11); lower Messinian samples in the central valleys (samples 12 and 13 near L'Aquila and samples 20–23 to the south); lower Messinian samples to the north (samples 14–19 at Monte Gorzano in the Laga Mountains) and to the south (samples 24–28 in Molise) of the easternmost massifs.

We collected 3–10 kg of rock per sample, which were processed at ETH Zurich, Switzerland, according to standard samples preparation and analytical techniques that are described in detail in the supplemental material. For the AFT thermochronometry, we analyzed all countable

TABLE 1. SAMPLE INFORMATION: COORDINATES, ELEVATION, DEPOSITIONAL AGE, CLOSEST VITRINITE DATA (RO), AND GEOLOGIC UNIT

N.	Sample name	Latitude (°N)	Longitude (°W)	Elevation (m ASL)	Deposition age (Ma)	Ro (%)	Geological formation name
1	TYR15	42.0479	13.9359	27	94–72	–	Pietraforte Formation
2	CIR62	41.2247	13.0901	2	23–20	–	San Felice Flysch
3	FAG69	41.5811	13.1082	850	34–23	–	Subligurian Unit
4	OLE20	41.8853	13.0494	505	8.4–7.3	0.33 ± 0.05	Frosinone Unit
5	SGU12	41.6638	13.1764	243	8.4–7.3	0.29 ± 0.03	Frosinone Unit
6	GTA05	41.6072	13.3876	232	8.4–7.3	0.31 ± 0.03	Frosinone Unit
7	GTA03	41.2804	13.7274	101	8.4–7.3	0.31 ± 0.03	Frosinone Unit
8	ARS06	42.1324	13.1503	844	7.1–6	0.30 ± 0.06	Argillosa Arenacea Unit
9	ARS07	42.1299	13.0224	577	7.1–6	0.30 ± 0.06	Argillosa Arenacea Unit
10	SOR19	41.8022	13.5384	641	7.1–6	0.31 ± 0.05	Argillosa Arenacea Unit
11	GTA04	41.6477	13.8016	814	7.1–6	0.37	Argillosa Arenacea Unit
12	COL63	42.2955	13.3391	941	7.1–6	0.46 ± 0.01	Argillosa Arenacea Unit
13	LAG42	42.5111	13.1613	811	7.1–6	0.46 ± 0.02	Laga Formation
14	GOR50	42.6286	13.3759	1572	7.1–6	0.46 ± 0.07	Laga Formation
15	GOR51	42.6271	13.3773	1655	7.1–6	0.46 ± 0.07	Laga Formation
16	GOR52	42.6244	13.3771	1812	7.1–6	0.46 ± 0.07	Laga Formation
17	GOR53	42.623	13.3757	1880	7.1–6	0.46 ± 0.07	Laga Formation
18	GOR54	42.6194	13.3788	2099	7.1–6	0.46 ± 0.07	Laga Formation
19	GOR55	42.619	13.3809	2154	7.1–6	0.46 ± 0.07	Laga Formation
20	MAI38	41.7626	13.9829	979	7.1–6	0.37 ± 0.07	Argillosa Arenacea Unit
21	MOL30	41.6222	14.0574	602	7.1–6	0.44 ± 0.11	Agnone Formation
22	MOL23	41.5085	14.3832	672	7.1–6	0.41 ± 0.03	Agnone Formation
23	MOL24	41.5254	14.3922	550	7.1–6	0.41 ± 0.03	Agnone Formation
24	MOL27	41.6803	14.2232	590	7.1–6	0.41 ± 0.03	Agnone Formation
25	MOL28	41.8217	14.1891	823	7.1–6	0.43 ± 0.01	Agnone Formation
26	MOL25	41.5344	14.456	561	7.1–6	0.41 ± 0.03	Agnone Formation
27	AGN31	41.7654	14.4005	598	7.1–6	0.44 ± 0.01	Agnone Formation
28	AGN33	41.8049	14.4188	804	7.1–6	0.44 ± 0.01	Agnone Formation

Notes: N. is the sample number as indicated in Fig. 1; Sample name is the label as given in the field.  
m ASL—meters above sea level.

grains (20–32 per samples) to maximize the total number of spontaneous tracks, which largely control the AFT analytical error, and to have the widest possible distribution of grain ages. Measurable horizontal confined track lengths were nearly absent and were not measured as their number would be largely insufficient for any modeling. For AHe thermochronometry, we picked up to six single apatite crystals per sample, based on the following characteristics ranked by priority: grain size >60 µm, no inclusions, simple geometrical form (avoiding broken crystals), no coating/surface abrasion. When available, we chose the biggest grains with no fractures nor inclusions, and perfect bipyramidal hexagonal shape. When optimal grains were not available, we prioritized: size >60 µm, purity (no inclusions), no internal fractures, and absence of broken tips. Each apatite was photographed and measured to calculate the alpha-ejection factor (Ft).

### 3.3. Method Principles and Quantification of Cooling Histories

For standard apatite composition, the AFT and AHe thermochronometers have nominal closure temperatures in the range of 50–70 °C and 100–120 °C, respectively, (Reiners and Brandon, 2006) which assuming a surface temperature of 10 °C and a steady geothermal gradient of 30

°C/km in the upper crust, correspond to a closure depth of ≤2 km for the AHe system and of <4 km for the AFT system. In order to fully reset the cooling age of detrital apatites by depositional or tectonic burial, temperatures higher than those of the AHe partial retention zone and of the AFT partial annealing zone, respectively, are necessary. The effective closure temperature also depends on the duration of burial: to fully reset a thermochronometric system, a short duration of burial requires higher temperatures. If burial conditions are such that no full thermal resetting is achieved, apatites retain partially or fully the cooling record of their earlier thermal history.

While temperature and time are the primary control factor on He retention and diffusion, the degree of radiation damage induced by the decay process also exerts a considerable control on diffusion kinetics; its effect is nonlinear (Gautheron et al., 2009). The radiation damage is primarily a function of the U and Th concentrations, of the time over which radiation damage is accumulated and of the thermal history of the sample as radiation damage can anneal with time. The effective U (eU) is commonly used as a proxy to account for the radiation damage due to the U and Th concentration (Flowers et al., 2009) and it is defined as  $eU = U + 0.235 \times Th$ , where U and Th are the concentration in ppm (Gautheron et al., 2009). The composition of apatite affects the kinetics of fission-track annealing and it also

affects how apatite responds to the etch procedure such that the diameter of the spontaneous tracks after etching (Dpar, see footnote 1) can be used to constrain the kinetic parameters of AFT annealing (Carlson et al., 1999).

Although it is possible to calculate effective closure temperatures for a given set of kinetic parameters and for a known cooling rate, this involves a number of approximations, including the assumption of monotonic cooling at a near-constant rate. Where there is the potential for a complex cooling history, for example, with detrital samples that may not have been fully reset, it can be helpful to perform thermal modeling for age prediction. We performed thermal modeling using the QTQt code from Gallagher (2012), which uses a Markov-Chain Monte-Carlo method to infer for a collection of grain ages with individual kinetic parameters, the most-likely time-temperature path that best predicts the measured data (and kinetic parameters) according to the applied diffusion and annealing models. For use in this model, age data can be treated as co-located, i.e., a single sample with multiple grains or can consist of multiple samples, assumed to have a common exhumation history, but separated by elevation, which provides a time lag based on vertical distance. We analyzed three samples and the Monte Gorzano age-elevation transect, and obtained temperature histories subject to two temperature constraints: temperature of ~40 °C at the depositional age of the detrital samples and a present-day temperature of  $10 \pm 10$  °C. For the age-elevation transect, we assume an initial geothermal gradient of 30 °C/km and 5 °C as the modern surface temperature difference given a maximum elevation difference between samples of 600 m. The input modeling parameters and data are detailed in the supplemental material.

## 4. RESULTS

### 4.1. Cooling Ages

Single grain AHe ages and mean sample AHe ages are reported in Table S1 in the supplemental material<sup>1</sup>. AFT data are reported in Tables S2 to S3 and plotted in Figures S1 to S2 in the supplemental material (see footnote 1). Thermal modeling results are shown in Figure 4 and discussed in section 5.1.2. The analytical error of our AHe

<sup>1</sup>Supplemental Material. Full descriptions of the analytical and modelling procedures together with tables and figures that report and illustrate the data details and the modelling inputs. Please visit <https://doi.org/10.1130/GSAB.S.16850296> to access the supplemental material, and contact editing@geosociety.org with any questions.

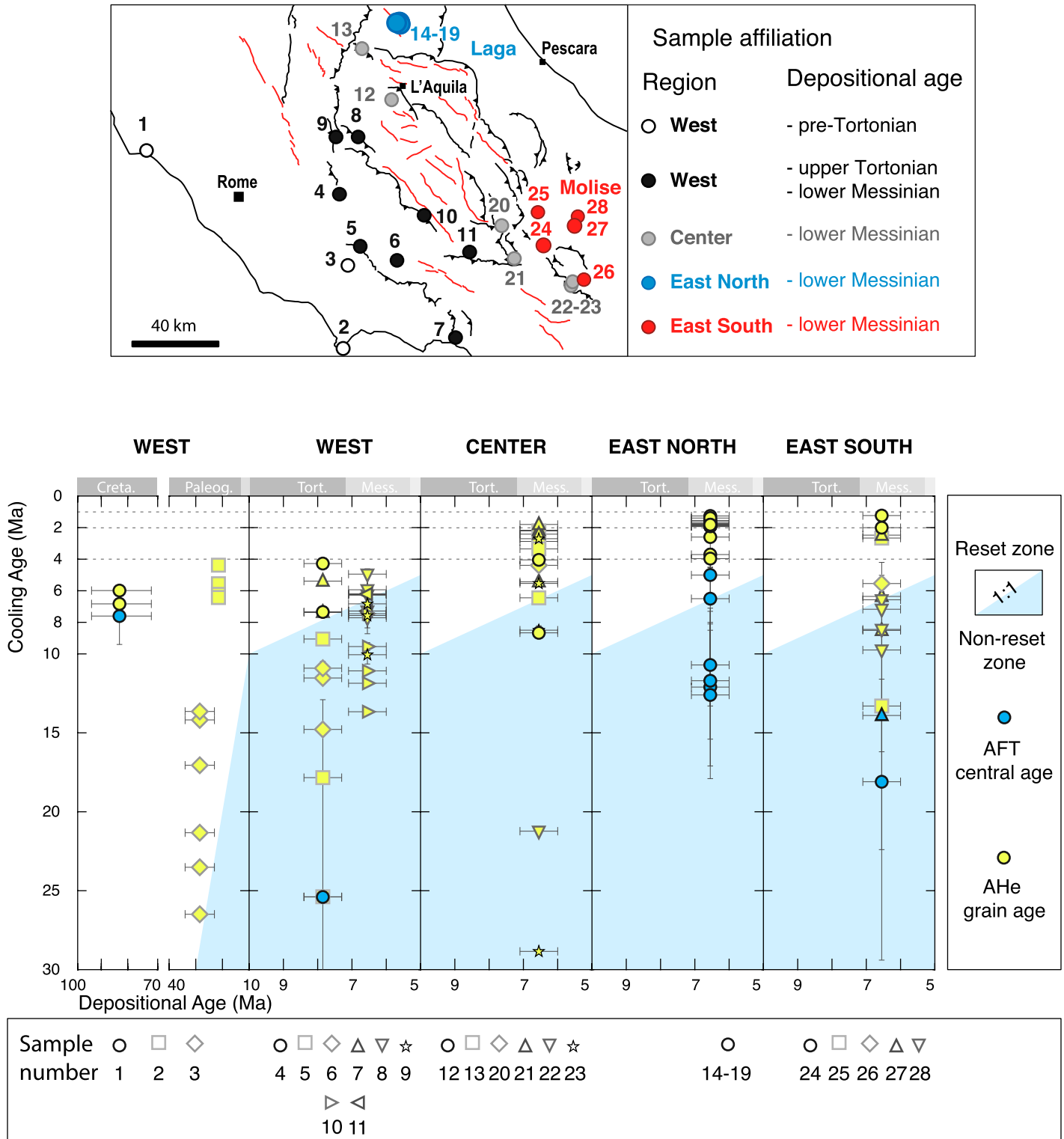


**Figure 3.** Simplified map of the study area in the central Apennines of Italy showing the subdivision of the dated samples in five groups based on their position and plot of depositional age versus cooling age of the dated samples. In the depositional age-cooling age plot, the vertical bar for each data point represents the analytical uncertainty of apatite (U-Th-Sm)/He (AHe) single grain ages and the standard error of central apatite fission-track (AFT) ages; the horizontal bar represents the depositional age range. For most samples, the uncertainty of the AHe grain ages, which is generally <10%, is smaller than the age symbol and in these cases the age symbol masks the uncertainty. We consider as fully reset the cooling ages that are younger than the depositional age range. Samples are plotted here relative to the minimum depositional age, which is where the 1:1 line passes through.

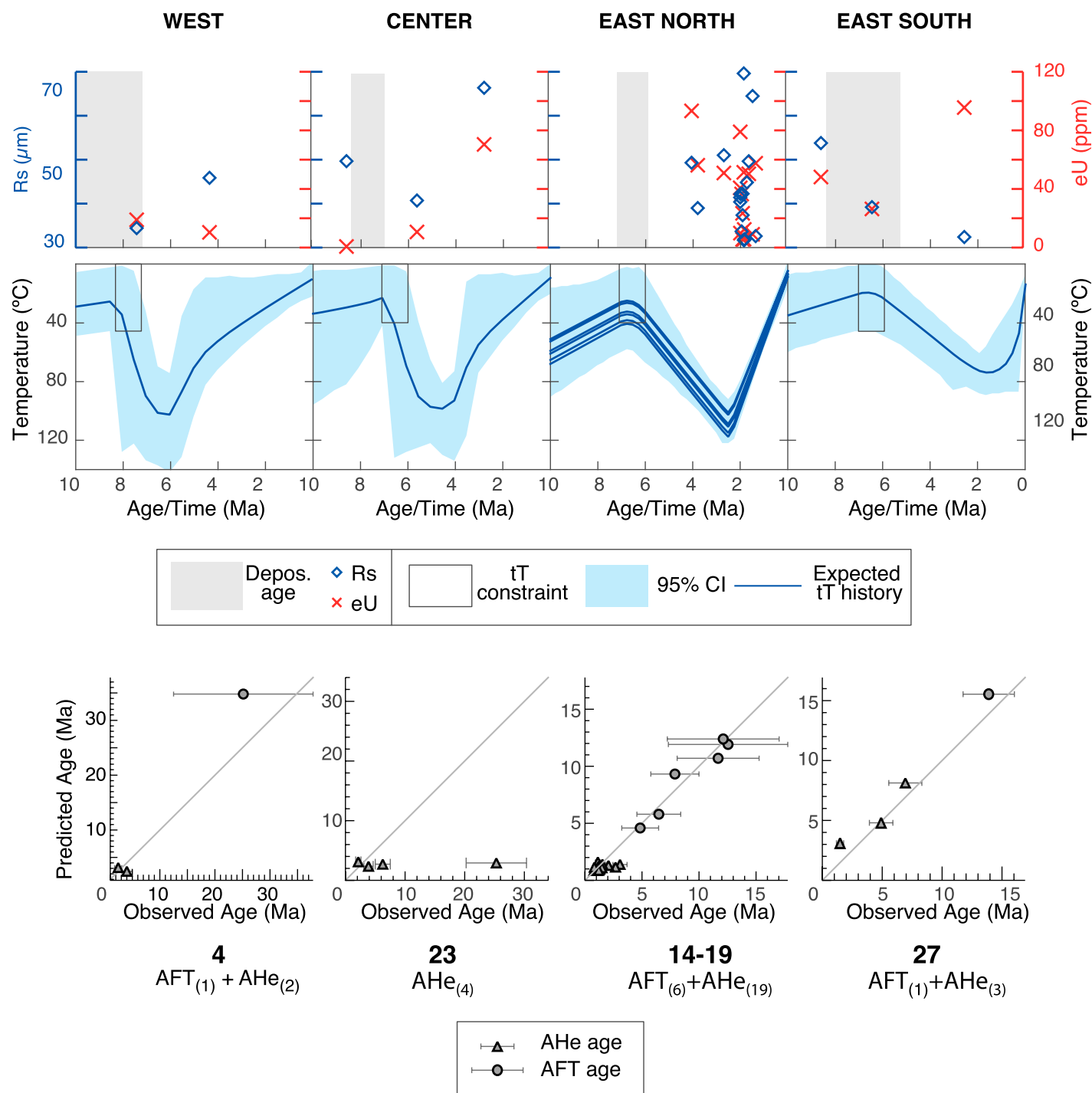


**Figure 4.** Thermal modeling results based on QTQt (Gallagher, 2012) for four groups of ages. Each group is referred to a region (west, center, east north, east south) within the central Apennines of Italy as defined in Fig. 3.  $R_s$  is the equivalent spherical radius of the dated grains and  $eU$  is the effective Uranium ( $eU = U + 0.235 \times Th$ ) that is a proxy for radiation damage; Gautheron et al., 2009). Depos. age indicates the age range of the depositional age. Time-temperature plots show the resulting expected time-temperature path (blue line) with its 95% confidence interval (CI) (light-blue area). tT constraint is the input time-temperature constraints that correspond to the depositional age and to temperatures below 40  $^{\circ}\text{C}$ . Modeling results are also plotted as observed versus predicted ages. Numbers in bold font are sample number and subscript numbers between parenthesis indicate the number of thermochronologic data for each sample. AFT—apatite fission-track; AHe—AHe- apatite (U-Th-Sm)/He.



grain ages is generally <10% with the exception of 10 grains out of 87 that have very high analytical error due to low He yield combined with low U and Th concentrations (Table S1). In this text, we refer to single grain AHe ages without specifying the analytical uncertainty and, instead, we report mean AHe ages with standard deviations at 68% confidence level and central AFT ages with uncertainty at 95% confidence level. Overall, single grain AHe ages range from 1 to 109 Ma, and AFT central ages range from  $5 \pm 1.7$  to  $25 \pm 13$  Ma.

To discriminate between reset and non-reset samples, we compare their cooling age to their depositional age: we define as reset the samples whose single grain ages (for AHe) or central age (for AFT) are younger than the minimum depositional age (Table 1; Fig. 3).

We recognize five regions across the study area where ages appear to have common characteristics and individual grain ages are compiled into these regional groupings in Figure 3. Fully reset samples are located close to the Tyrrhenian coast, where samples 1 and 2 have reset single grain AHe ages in the range between 6.8 and 4.4 Ma and a reset central AFT age of  $7.6 \pm 1.8$  Ma. The remaining samples in the western sector of the study area (samples 3–11) include a non-reset central AFT age and AHe grain ages that straddle the depositional age indicating a variable degree of age resetting (Fig. 3).

In the central sector of the study area, three AHe samples (samples 13, 20, and 21) are potentially fully reset: two samples each have four dated grains with mean AHe ages of  $3.7 \pm 1.9$  Ma and  $3.0 \pm 1.7$  Ma, respectively, and one sample has only one 4.4 Ma old AHe grain. In sample 13, one AHe grain age is actually older than the minimum depositional age for this sample, which can be estimated as having a minimum age of 6 Ma. However, based on the stratigraphic position of this sample, its depositional age is likely closer to 7 Ma than to 6 Ma and therefore we consider it as most likely fully reset. The remaining samples (12, 22, and 23) have AHe ages varying over a wide range from older to younger than the depositional age.

In the eastern sector of the study area, among the samples from the age-elevation profile at Monte Gorzano in the Laga Mountains (samples 14–19; Figs. S1 and S3 in the supplemental material), the lowest elevation AFT ages ( $5.0 \pm 1.7$  Ma and  $6.5 \pm 2.0$  Ma) are partially to fully reset, the remaining AFT ages are partially to non-reset, all the AHe grain ages are fully reset and range between 4.0 and 1.4 Ma.

In the Molise hills, samples 24 and 25 both have potentially fully reset AHe ages although only three grains in total could be dated resulting in AHe ages between 2.7 and 1.2 Ma. The

remaining AHe grain ages vary in each sample over a relatively wide range indicating variable resetting degree and all three AFT ages are non-reset (Fig. 3).

## 5. DISCUSSION

### 5.1. Variability of Results

#### 5.1.1. Age Dispersion and Degree of Resetting

Sources of dispersion and uncertainty of AHe ages can be attributed to several factors: He-bearing inclusions, possibly overlooked during picking that can give old outlier grain ages (MOL24a2, MOL30a1, and LAG42a2 in Table S1 in the supplemental material); Ft correction, that is limited in the case of irregular or broken grain shapes as is often the case in sedimentary samples; U and Th zoning, that can result in older ages in the case of U-rich grain boundaries (Hourigan et al., 2005); absent U-rich neighbors, that can implant He in U-poor apatites (Spiegel et al., 2009); and partial resetting of detrital grains with different pre-depositional ages (Fox et al., 2019). For both AHe and AFT ages, a major factor controlling the age dispersion is the thermal history of the dated samples, which can result in very different grain ages either in the case of slow cooling or of cooling from maximum temperatures close to closure temperature. With thermal modeling we can largely account for some of these factors like cooling rate and partial resetting, but to be most meaningful, additional constraints are generally needed. A constraint is provided by the depositional age of the sampled sediments which indicates that the sample was at surface temperatures at that time. However, due to the scatter and the uncertainty of the cooling ages as well as the uncertainty of the depositional age, caution is necessary when defining the degree of resetting based on comparison to the depositional age, especially when only a few grains per sample are available. In this case, it is important to use additional proxies for burial conditions as, for instance, Ro data that are available in our study area and that are discussed below together with modeling results.

#### 5.1.2. Thermal Modeling

Complex thermal histories involving reheating by burial after a first phase of pre-depositional cooling and a second phase of post-depositional exhumational-cooling result in a complex relationship between age and closure to daughter product loss. The measured age for samples that are partially reset may not reflect a key time of cooling, but rather reflects continuous, but incomplete He loss at elevated temperatures for extended periods of time. The thermal modeling provided by QTQt permits us to incor-

porate the grain-specific retention and annealing characteristics, as well as complex thermal histories, and these histories can be integrated to determine the age. It is important to calibrate models with independent geological and thermal data to discriminate between scenarios. Ro data can be input into QTQt and can be modeled together with the thermochronologic ages. However, as our thermochronologic samples are not co-located with the Ro data and as their exact stratigraphic position relative to the available Ro data is difficult to reconstruct, we opted to use Ro data to validate the thermal modeling results rather than to constrain them. Ro data, if converted to corresponding temperatures, can be compared to the modeled maximum burial temperatures derived from cooling ages. For the Ro-temperature conversion, we refer to a burial study in a similar context that is in the Miocene turbiditic deposits of the Northern Apennines, where Ro and AFT data have been calibrated against each other (Zattin et al., 2002). There, Ro values of 0.29% correspond to temperatures of 75 °C and Ro values of 0.43%–0.44% to a temperature of 95 °C.

There are four groups of ages that we regarded as inclusive of sufficient AHe and AFT constraints to warrant modeling of non-monotonous thermal histories using QTQt (Fig. 4). Three groups consist of one sample each that have spread in grain ages (sample 23) or have both AFT and AHe ages (samples 4 and 27); a fourth group comprises six samples along an elevation profile. For sample 4, the model indicates burial until ca. 6 Ma followed by relatively rapid cooling until 4 Ma to a low temperature (Fig. 4). Close to sample 4, Ro values are ~0.33% and the modeled path indicates a maximum temperature close to 100 °C. However, paths to a maximum temperature of 80 °C are also likely according to the model and therefore the modeled time-temperature path can be considered acceptable.

Among the four AHe ages we obtained for sample 23, two are younger than the depositional age and three show a good correlation between age and eU (Fig. 4), which could indicate an effect of radiation damage on He diffusion. The fourth grain age was large and difficult to fit with any thermal model. The modeled path for this sample indicates maximum burial temperatures of >90 °C between 4 and 6 Ma. Vitrinite data close to this sample are 0.41%, which indicate temperatures close to 90 °C. Maximum temperatures are followed by cooling to temperatures below 40 °C after 4 Ma.

The Monte Gorzano age-elevation transect includes AFT ages that are clearly unreset, but also some individual AFT grain ages that might be reset (Figs. S1 and S3 in the supplemental

material) as well as reset AHe grains (Fig. 4). This combination requires that post-depositional heating be rapid and short-lived so as to reset the He ages, and not the fission track ages. This emerged from the models as rapid heating from 6 to nearly 2 Ma reaching a peak temperature of over 120 °C, followed by rapid cooling to the modern surface. Although 120 °C would generally be regarded as over the AFT closure temperature, the short duration of heating resulted in only partially reset AFT ages. The maximum temperature of close to 120 °C, is consistent with the Ro value of 0.46% and with ~4 km thickness estimates for the Laga Formation (Milli et al., 2013).

Vitrinite reflectance data in proximity of sample 27 give quite high Ro values of 0.44%. However, the AFT age of this sample is non-reset and some AHe ages of this sample are older than the depositional age and they have a clear positive correlation between ages and spherical radius indicating sensitivity to diffusion properties (Fig. 4). The thermal history derived from the model indicates maximum temperatures below 90 °C and within the AHe partial retention zone until ca. 2 Ma followed by rapid cooling to surface temperatures.

## 5.2. Thermotectonic Evolution of the Central Apennines

### 5.2.1. Migrating Cooling From West to East

In the central Apennines, cooling ages decrease from west to east (Figs. 3 and 5): the youngest AHe grain ages are  $\leq 4$  Ma in the western sector, close to 2 Ma in the central and north-eastern sectors and as young as 1–2 Ma in the southeastern region. The cooling paths for the modeled partially reset samples (Fig. 4) show onset of cooling after 6 Ma for the sample in the west, after 4 Ma for the sample in the center, after 2.5 Ma in the Laga Mountains and after 2 Ma in Molise. Fully reset AFT ages are found in the west along the Tyrrhenian coast and in the northeast in the Laga Mountains indicating that exhumation from depth of  $\geq 3$  km only occurred in these areas.

By combining the time-temperature paths inferred by modeling individual grain ages with the time-temperature inference from the potentially fully reset samples, it is possible to illustrate how cooling progressed from west to east across the central Apennines (Fig. 5). For the fully reset samples, the nominal closure temperature, corrected for the grain size in the case of AHe ages, and assuming a cooling rate of 10 °C/km, provides an estimate of temperature at the age. These calculations are summarized by showing the temperature at which the samples resided at discrete times from 6 Ma to present

(Fig. 5). This analysis indicates that the samples along the Tyrrhenian coast cooled at temperatures below 100 °C prior to 6 Ma, and at 4 Ma they were already at temperatures below 60 °C. The samples in the east were cooling below 100 °C (samples 14–19) or 60 °C (samples 13 and 20–27) only after 2 Ma.

### 5.2.2. Late Tortonian–Early Pliocene Cooling in the West

Along the Tyrrhenian coast, our oldest fully reset ages indicate rapid cooling from temperatures of  $\geq 120$  °C (AFT nominal closure temperature; depths of  $\geq 3$  km) to  $\sim 70$  °C in the late Tortonian–Messinian (samples 1 and 2; Figs. 1, 2, and 5), well before the onset of the volcanic activity near Rome. This indicates that these ages were not affected by the current high heat flux (Chiodini et al., 2013) in this region as the sampled rocks were near the surface before the increase in heat flux. During the late Tortonian, offshore normal faults related to back-arc extension were active, the Volsci range was in a wedge-top position (Cosentino et al., 2003, 2010), the frontal thrust was active at the front of this range and therefore the Tyrrhenian coast region was internal to the wedge. Normal faulting has been observed close to sample 2, with onset during the Tortonian–early Messinian and ongoing until the late Messinian (Cipollari et al., 1999b). By the late Messinian, extensional basins along the shore were actively filling with clastic sediments (Faccenna et al., 1994; Cipollari et al., 1999a; Cosentino et al., 2006). Thus, the 8–6 Ma exhumation event as recorded by our cooling ages along the Tyrrhenian coast can be interpreted as related to the onset of extension in this region.

Samples from the upper Tortonian foredeep basin (samples 4–7) and from the most internal lower Messinian foredeep basin (samples 8–11) indicate cooling to temperatures below 80–60 °C no later than 4 Ma (Fig. 4). The onset time of cooling is not resolved by the cooling ages and it is constrained only by the minimum depositional age for these samples, which is 7.3 Ma and 6 Ma for the upper Tortonian and lower Messinian samples, respectively. The time interval between 7.3 and 4 Ma overlaps with the last phases of thrusting recorded in the region from the Volsci to the Simbruini–Ernici ranges (Fig. 2). The low resetting degree of the samples from these units can be related to the combined effect of little burial and short residence time at depth. Estimates for the maximum thickness of the foredeep sandstones in the Latina and Roveto valleys do not exceed 2 km (Cosentino et al., 2003) and burial may have lasted  $\leq 1$  m.y. if the onset time for cooling is close to the minimum depositional age.

In summary, cooling during the late Tortonian–Messinian is recorded along the Tyrrhenian coast in relation to the opening of the extensional basin that caused exhumation from depths of  $\geq 3$  km. Inland, in the western sector of the central Apennines, Messinian–earliest Pliocene cooling from very shallow depths may have occurred in relation to the latest phases of thrusting, when sections of the foredeep shifted to a wedge-top position with local exposure and erosion of the thrust hanging walls.

### 5.2.3. Pliocene-to-Pleistocene Cooling in the Center and East

Samples from the central sector of the study area (samples 12, 13, and 20–23) are from the early Messinian foredeep and show a large fraction of reset AHe ages (Fig. 3). Thermal modeling of one of the partially reset samples (sample 23, Fig. 4) indicates that cooling occurred after 4 Ma. This suggests that at least locally cooling may have started during the last phases of Pliocene thrusting (Fig. 2). However, the fact that a large fraction of AHe grain ages occur at ca. 2 Ma suggests that cooling from  $\sim 2$  km depth continued with the onset of the extensional deformation as inferred from the stratigraphic record of the intermontane basins of this region (Figs. 2 and 5).

In the Laga Mountains, the Monte Gorzano age-elevation transect (samples 14–19; Fig. S1 in the supplemental material) is in the footwall of an active normal fault (Porreca et al., 2018; Fig. 1). The AFT ages on the elevation traverse contributed little to the thermal history determination, given that they were non-reset or partially reset. The fully reset AHe ages center at ca. 2 Ma and thermal modeling indicates that cooling from temperatures of  $\geq 120$  °C did not start until ca. 2.5 Ma.

In Molise, partially to fully reset ages as young as  $\geq 1$  Ma are from lower Messinian sediments that were over-thrust by the far-traveled Sicilide units, which represent upper Messinian–lower Pliocene wedge-top basins (Cosentino et al., 2018). In this region, intermontane basin are not present and cooling might have started during the Pleistocene, as indicated by the thermal modeling of one of the partially reset samples.

## 5.3. Implications for Timing and Mechanisms of Orogenic Topography

The rock cooling histories derived from thermochronometry combined with the stratigraphic information from the Apenninic tectonic basins provide an integrated picture of orogenesis, topographic uplift, and exhumation. The underlying process is subduction and trench retreat leading to an eastward migrating wave of contractional

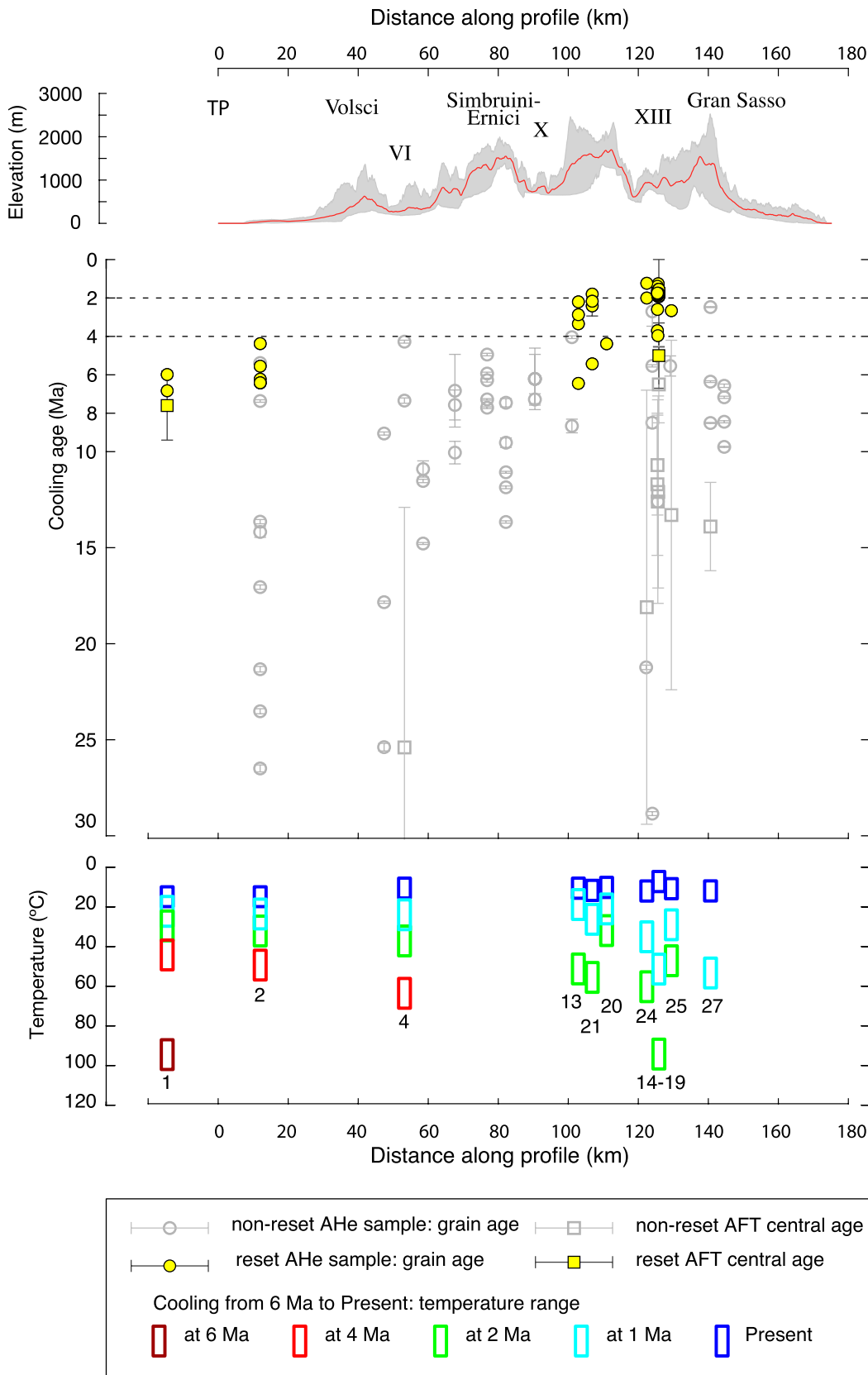


**Figure 5.** Above: topographic swath profiles across the central Apennines of Italy with mean elevation indicated by a red line within a gray envelope representing minimum and maximum elevation. The location of the profile trace is shown in Figure 1 (TP). Middle: cooling ages from this study projected along the trace of the topographic profile. Below: temperature at different times for the modeled samples shown in Figure 6 (samples 4, 14–19, 23, and 27) and for the fully reset samples (samples 1, 2, 13, 20, 21, 24, and 25). The temperature range box for the past times represents the temperature  $\pm 7.5^\circ\text{C}$  derived from the cooling rate as in the thermal models of Figure 6 or from the nominal closure temperatures for the fully reset samples. For the apatite (U-Th-Sm)/He grain ages, the nominal closure temperature was corrected for grain size and averaged within each sample. The temperature range box for the Present is the modern surface temperature at the sample elevation  $\pm 5^\circ\text{C}$  derived from a lapse rate of  $5^\circ\text{C}/\text{km}$  and a surface temperature at sea level of  $15^\circ\text{C}$ . AHe—apatite (U-Th-Sm)/He; AFT—apatite fission-track.

deformation followed by a later phase of extensional deformation. The onset of contractional deformation propagated from the Tyrrhenian coast to the Adriatic piedmont from ca. 9 Ma to ca. 3.5 Ma (Fig. 2). Contractional deformation in the west is documented in marine basins, but cooling prior to 5 Ma indicates local erosion and exhumation during contraction. The transition from marine to exclusively terrestrial deposition marking widespread surface uplift occurred later (ca. 3 Ma), is nearly contemporaneously across the central Apennines, and is associated with the onset of extensional deformation (Fig. 2). Our results from the central and eastern regions do not resolve early cooling, but show rapid cooling, initiating at or just prior to 3 Ma (Figs. 4 and 5), contemporaneous with the formation of extensional basins (Fig. 2). By the late Pliocene–early Pleistocene, the topography of the central Apennines started to increase significantly at the long-wavelength (San Jose et al., 2020), and

extensional faults were actively bounding continental, intermontane basins (Cavinato et al., 1994; Cosentino et al., 2009, 2017). In the north-east of the study area (Laga Mountains), thermochronologic data resolve the onset of fast and significant extensional exhumation in the order of ~4 km at the footwall of normal faults that are still active today (Porreca et al., 2018; Figs. 1 and 4). In the late Gelasian, at ca. 2 Ma, widespread cooling is resolved throughout the central Apennines (Figs. 2, 3, and 5) with additional evidence of erosion provided by large angular unconformities and abandonment surfaces formed from Rome to L'Aquila (Cosentino et al., 2017). Thus, from our reconstructions it is evident that during the Plio-Pleistocene, eastward propagation of extensional deformation and associated uplift and exhumation was not at a steady rate.

These observations altogether call for a change in the subduction dynamics between the late Miocene to the modern. Until the latest Mio-

cene or Pliocene, the subducting plate was continuous and its retreat drove the eastward propagation of both frontal contraction and upper plate extension (Fig. 6). In the late Pliocene and Pleistocene, we see widespread surface uplift of the central Apennines, with accelerated erosion and exhumation, all associated with extensional tectonics (Fig. 6). Indeed, in the late Pliocene and Pleistocene, extension did not migrate eastward following contraction as when slab roll back was active and, paradoxically, it occurred at the same time as the rise of surface topography rather than with its subsidence as previously proposed (Cavinato and DeCelles, 1999). The western regions of the central Apennines preserve a Pleistocene paleoshoreline, 10–100 km long (VII: Tiberino Basin, Figs. 1 and 2; Mancini et al., 2007; Cosentino et al., 2017), which is almost unperturbed by extensional faults (D'Agostino et al., 2001). However, in the eastern regions, we document since the Piacenzian ~4 km of exhu-

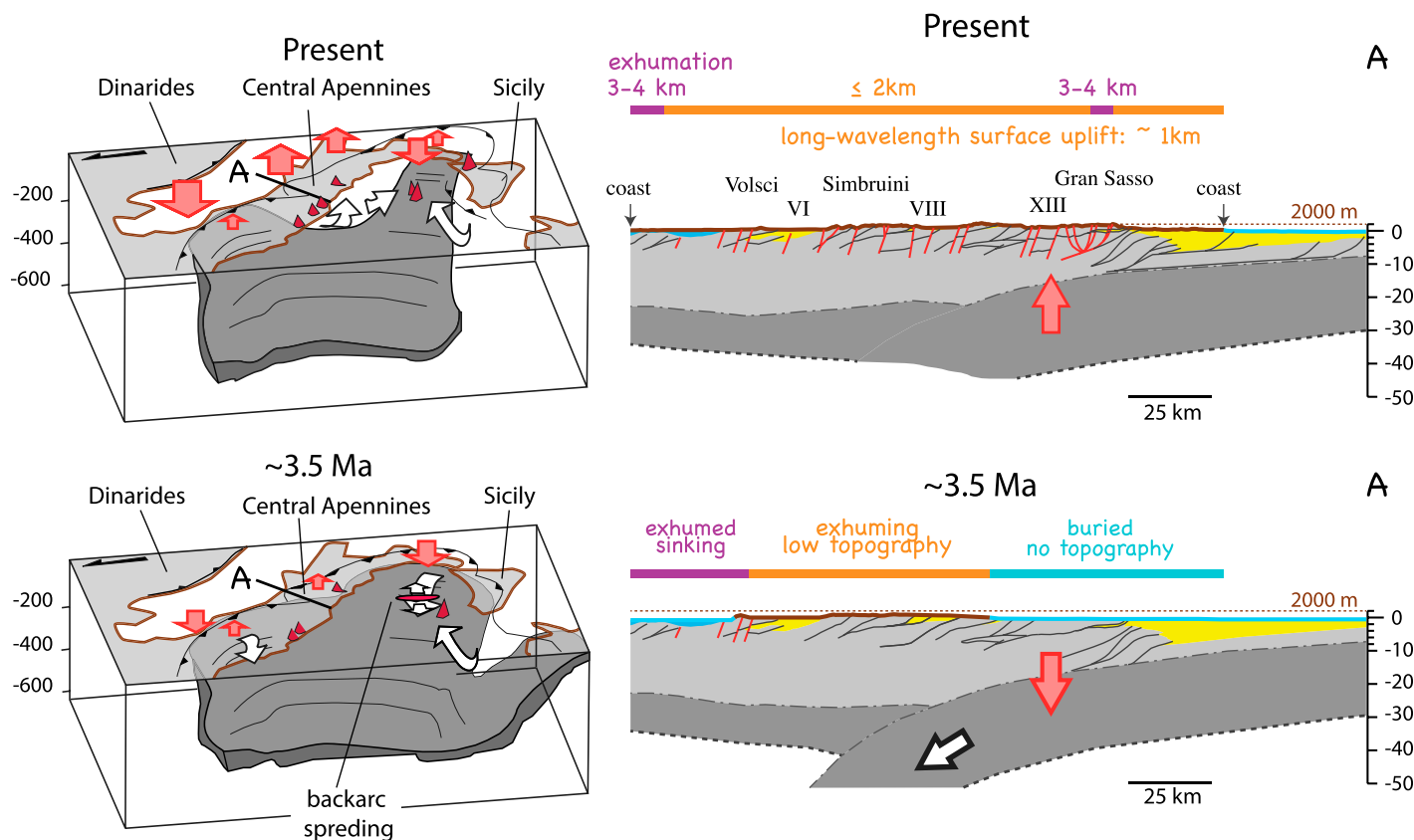


**Figure 6.** Two stage interpretative scenario for the evolution of the central Apennines of Italy showing the relation between deformation and surface uplift within the orogenic wedge and the dynamic of the subduction system: from the late Tortonian to the Piacenzian the continuous slab-roll back caused forelandward migration of the wedge contracting at the front and extending at the rear with limited topographic growth; from the Piacenzian to the present, local slab detachment caused the opening of extensional intermontane across the central Apennines from the west to the east, exhumation from depths of >3–4 km in the north east and prominent topographic growth. The 3D scheme of the Apenninic subduction system is modified from Faccenna et al. (2014). Red arrows indicate the direction of surface motion. White arrows indicate the motion of the subducting plate and of mantle flows. The cross-section across the central Apennines is adapted from Cosentino et al. (2010).

mation at the footwall of a normal fault that generated significant local surface uplift (~1.5 km high relief; Fig. 1, section A). Thus, during the Plio-Pleistocene although some contraction has continued in the Adriatic (e.g., Patacca and Scandone, 1989), in the central Apennines the pattern of deformation associated with retreating subduction was disrupted and replaced by one of uplift and widespread extension. Among the mechanisms so far proposed as controlling the upper plate dynamics of the central Apennines since the late Pliocene, only a local slab detachment is consistent with geophysical data and can sustain both extension and large scale 1–2 km high, regional surface uplift (e.g., Wortel and Spakman, 2000; Gvirtzman and Nur, 2001; Faure Walker et al., 2012; Faccenna et al., 2014).

#### 5.4. Surface Uplift and Extension in the Central and Northern Apennines

Northern and central Apennines share many similarities in terms of tectonic history. Some of the most striking similarities are the timing of exhumation and its pattern across the strike of the orogen, from SW to NE. In fact, between 7 and 4 Ma, a major phase of extensional exhumation affects the Tyrrhenian regions of both the Northern (e.g., Fellin et al., 2007) and the central Apennines (Figs. 2 and 5). Moreover, also in the Northern Apennines, the youngest ages are on the Adriatic side of the orogen, where they are typically close to 2–1 Ma, and exhumation migrated from west to east (e.g., Thomson et al., 2010). However, in the Northern Apennines, young cooling ages (1–2 Ma), close to the main drainage divide are related to exhumation along normal faults but farther to the east, they are related to frontal accretion and possibly also to underplating of foreland sediments and not to extensional deformation (Thomson et al., 2010). In the central Apennines, the youngest and easternmost cooling ages are: (a) in the Laga Mountains, where extension is still active today and where they are clearly associated with exhumation of a normal fault footwall, and (b) in the Molise hills, where there is no clear record of extension and where the 1–2 Ma cooling ages could be associated with surface uplift either at the regional scale, as along the Adriatic Piedmont east of Gran Sasso (XVI, Figs. 1 and 2), or to late Pliocene–early Pleistocene contractional deformation (Vezzani et al., 2010). However, a major difference between the Northern and central Apennines is in the time of uplift above sea level. In the Northern Apennines, despite a rather complex paleogeographic scenario at the transition between Messinian and Pliocene, the first non-marine sediments in intermontane, post-rift, extensional basins date back to the lower Plio-

cene in the west and to the upper Pliocene in the east (e.g., Conti et al., 2020 and references therein). Cooling ages in the Northern Apennines are consistent with eastward migration of exhumation associated with extensional faults between the late Miocene and the Pliocene–early Pleistocene (Thomson et al., 2010). This suggests that, differently from what we observe in the central Apennines, in the Northern Apennines, extension and uplift above sea level did not occur at the same time in the west and in the east but they migrated eastward at least through the Pliocene–early Pleistocene. Thus, the concurrence of the onset of extension and of surface uplift above sea level during the late Pliocene across the central Apennines, in the west and in the east, is a unique feature of this region that it is not observed in the Northern Apennines.

The central and Northern Apennines differ fundamentally in their present state: whereas in the Northern Apennines, subduction is still active and the stress regime at the front is clearly compressive, in the central Apennines there is no clear evidence of either active subduction or compressive stress regime (Montone et al., 2004; Faccenna et al., 2014 and reference therein). Finally, in the Northern Apennines several lines of evidence indicate the Pleistocene–Quaternary as a time when a pulse of surface uplift might have occurred at the regional scale (e.g., Argnani et al., 2003). However, along the front of the Northern Apennines, well-dated fluvial sediments indicate that the Pleistocene–Quaternary surface uplift is related to active blind thrust buried in the Po Plain (Picotti and Pazzaglia, 2008). Moreover, in the Northern Apennines the Pleistocene–Quaternary pulse of uplift would have occurred after the first pulse of eastward-migrating surface uplift and after the onset of extension and wide surface uplift observed in the central Apennines. Conclusively, although slab-break off has been proposed as a possible mechanism to explain a pulse of rapid surface uplift in the Northern Apennines (Carminati et al., 1999; Argnani et al., 2003), recent geophysical data support the idea that slab break off is localized rather beneath the central Apennines (e.g., Wortel and Spakman, 2000; Gvirtzman and Nur, 2001; Faure Walker et al., 2012; Faccenna et al., 2014) and our data support the view that the Adriatic slab detached beneath this area in the late Pliocene.

#### 6. CONCLUSIONS

In the central Apennines, new thermochronologic data, including 28 apatite (U-Th)/He and 10 apatite fission track ages, combined with stratigraphic data constraining syn-tectonic deformation and surface uplift, leads to the following conclusions:

- at ca. 8 and 5 Ma, along the Tyrrhenian coast, moderate topographic growth concurred with post-contractional cooling from depths of  $\geq 3$ –4 km in response to extensional deformation that led to the opening of marine rift basins;

- after 5 Ma, moderate topographic growth continued together with diachronous cooling from shallow depths of  $\leq 2$  km, between  $\leq 4$  Ma in the west and  $\leq 1$  Ma in the southeast, which occurred simultaneously with the late stages of foreland basin system deposition and thrust deformation, associated with subduction of the Adriatic plate;

- from ca. 2.5 Ma to the present, throughout the central Apennines, large regional topographic growth occurred simultaneously with the opening of extensional intermontane basins and with erosion and cooling from  $\leq 2$  km depths in the central region and from  $\geq 3$ –4 km depths in the northeastern region (Laga Mountains);

- these observations are consistent with detachment of the Adriatic slab beneath the central Apennines in the late Pliocene or early Pleistocene.

#### ACKNOWLEDGMENTS

The project was funded by the European Union's Horizon 2020 research and innovation program under the Marie Skłodowska-Curie grant agreement no. 674899. The grant to the Dipartimento di Scienze, Università degli Studi Roma Tre (MIUR—Ministero dell'Istruzione, dell'Università e della Ricerca) Italy Dipartimenti di Eccellenza, articolo 1, commi 314–337 legge 232/2016) is gratefully acknowledged.

#### REFERENCES CITED

- Aldega, L., Botti, F., and Corrado, S., 2007, Clay mineral assemblages and vitrinite reflectance in the Laga Basin (Central Apennines, Italy): What do they record? *Clays and Clay Minerals*, v. 55, p. 504–518, <https://doi.org/10.1346/CCMN.2007.0550505>.
- Argnani, A., Barbacini, G., Bernini, M., Camurri, F., Ghielmi, M., Papani, G., Rizzini, F., Rogledi, S., and Torelli, L., 2003, Gravity tectonics driven by Quaternary uplift in the Northern Apennines: insights from the LaSpezia-Reggio Emilia geo-transect: *Quaternary International*, v. 101–102, p. 13–26, [https://doi.org/10.1016/S1040-6182\(02\)00088-5](https://doi.org/10.1016/S1040-6182(02)00088-5).
- Bigi, S., Casero, P., and Ciotoli, G., 2011, Seismic interpretation of the Laga Basin: constraints on the structural setting and kinematics of the Central Apennines: *Journal of the Geological Society*, v. 168, p. 179–189, <https://doi.org/10.1144/0016-76492010-084>.
- Bigi, S., Conti, A., Casero, P., Ruggiero, L., Recanati, R., and Lipparini, L., 2013, Geological model of the central Periadriatic basin (Apennines, Italy): Marine and Petroleum Geology, v. 42, p. 107–121, <https://doi.org/10.1016/j.marpetgeo.2012.07.005>.
- Boccaletti, M., Calamita, F., Deiana, G., Gelati, R., Massari, F., Moratti, G., and Ricci Lucchi, F., 1990, Migrating foredeep-thrust belt system in the northern Apennines and southern Alps: Palaeogeography, Palaeoclimatology, Palaeoecology, v. 77, p. 3–14, [https://doi.org/10.1016/0031-0182\(90\)90095-O](https://doi.org/10.1016/0031-0182(90)90095-O).
- Cantalamesa, G., and Di Celma, C., 2004, Sequence response to syndepositional regional uplift: Insights from high-resolution sequence stratigraphy of late Early Pleistocene strata, Periadriatic Basin, central Italy: *Sedimentary Geology*, v. 164, p. 283–309, <https://doi.org/10.1016/j.sedgeo.2003.11.003>.



- Carlson, W.D., Donelick, R.A., and Ketcham, R.A., 1999, Variability of apatite fission-track annealing kinetics: I. Experimental results: *The American Mineralogist*, v. 84, p. 1213–1223, <https://doi.org/10.2138/am-1999-0901>.
- Carminati, E., Giunchi, C., Argani, A., Sabadini, R., and Fernandez, M., 1999, Plio-Quaternary vertical motion of the Northern Apennines: Insights from dynamic modeling: *Tectonics*, v. 18, p. 703–718, <https://doi.org/10.1029/1999TC900015>.
- Casero, P., 2004, Structural setting of petroleum exploration plays in Italy: Special Volume of the Italian Geological Society for the IGC 32, v. 107, p. 319–322.
- Cataldi, R., Mongelli, F., Squarci, P., Taffi, L., Zito, G., and Calore, C., 1995, Geothermal ranking of Italian territory: *Geothermics*, v. 24, p. 115–129, [https://doi.org/10.1016/0375-6505\(94\)00026-9](https://doi.org/10.1016/0375-6505(94)00026-9).
- Cavinato, G.P., and DeCelles, P., 1999, Extensional basins in the tectonically bimodal central Apennines fold-thrust belt, Italy: Response to corner flow above a subducting slab in retrograde motion: *Geology*, v. 27, p. 955–958, [https://doi.org/10.1130/0091-7613\(1999\)027<0955:EBITTB>2.3.CO;2](https://doi.org/10.1130/0091-7613(1999)027<0955:EBITTB>2.3.CO;2).
- Cavinato, G.P., Cosentino, D., De Rita, D., Funicello, R., and Parotto, M., 1994, Tectonic-sedimentary evolution of intraapenninic basins and correlation with the volcano-tectonic activity in Central Italy: *Memorie Descrittive della Carta Geologica d'Italia*, v. 49, p. 63–76.
- Cavinato, G.P., Carusi, C., Dall'Asta, M., Miccadei, E., and Piacentini, T., 2002, Sedimentary and tectonic evolution of Plio-Pleistocene alluvial and lacustrine deposits of Fucino Basin (central Italy): *Sedimentary Geology*, v. 148, p. 29–59, [https://doi.org/10.1016/S0037-0738\(01\)00209-3](https://doi.org/10.1016/S0037-0738(01)00209-3).
- Centamore, E., and Rossi, D., 2009, Neogene-Quaternary tectonics and sedimentation in the Central Apennines: *Italian Journal of Geosciences*, v. 128, p. 73–88.
- Centamore, E., Cantalamessa, G., Micarelli, A., Potetti, M., Berti, D., Bigi, S., Morelli, C., and Ridolfi, M., 1992, Stratigrafia e analisi di facies dei depositi del Miocene e del Pliocene inferiore dell'avanfossa marchigiano-abruzzese e delle zone limitrofe: *Studi Geologici Camerti*, volume speciale, v. 1991, no. 2, p. 125–131.
- Centamore, E., Crescenti, U., and Dramis, F., 2006a, Note Illustrative della Carta Geologica d'Italia alla scala 1:50,000, foglio 360-Torre de' Passeri: Servizio Geologico d'Italia, 128 p.
- Centamore, E., Crescenti, U., and Dramis, F., 2006b, Note Illustrative della Carta Geologica d'Italia alla scala 1:50,000, foglio 368-Avezzano: Servizio Geologico d'Italia, 119 p.
- Centamore, E., Crescenti, U., and Dramis, F., 2006c, Note Illustrative della Carta Geologica d'Italia alla scala 1:50,000, foglio 369-Sulmona: Servizio Geologico d'Italia, 154 p.
- CGI Terracina, 1960, Carta Geologica d'Italia Terracina foglio 170 della Carta dell'I.G.M.: Servizio Geologico d'Italia, scale 1:100,000.
- Chiarabba, C., Jovane, L., and Di Stefano, R., 2005, A new view of Italian seismicity using 20 years of instrumental recordings: *Tectonophysics*, v. 395, p. 251–268, <https://doi.org/10.1016/j.tecto.2004.09.013>.
- Chiodini, G., Cardellini, C., Caliro, S., Chiarabba, C., and Frondini, F., 2013, Advective heat transport associated with regional Earth degassing in central Apennine (Italy): *Earth and Planetary Science Letters*, v. 373, p. 65–74, <https://doi.org/10.1016/j.epsl.2013.04.009>.
- Cipollari, P., and Cosentino, D., 1992, La linea Olevano-Antrodocco: Contributo della biostratigrafia alla sua caratterizzazione cinematica: *Studi Geologici Camerti*, volume speciale, CROP, v. 11, p. 143–149.
- Cipollari, P., and Cosentino, D., 1993, Le Arenarie di Torrice: Un deposito di bacino di piggy-back del Messiniano nell'Appennino centrale: *Bollettino della Società Geologica Italiana*, v. 112, p. 497–505.
- Cipollari, P., and Cosentino, D., 1995a, Il sistema Tierreno-Appennino: Segmentazione litosferica e propagazione del fronte compressivo: *Studi Geologici Camerti*, volume speciale, v. 1995, no. 2, p. 125–134.
- Cipollari, P., and Cosentino, D., 1995b, Miocene unconformities in the Central Apennines: Geodynamic significance and sedimentary basin evolution: *Tectonophysics*, v. 252, p. 375–389, [https://doi.org/10.1016/0040-1951\(95\)00088-7](https://doi.org/10.1016/0040-1951(95)00088-7).
- Cipollari, P., Cosentino, D., Esu, D., Girotti, O., Gliozzi, E., and Praturion, A., 1999a, Thrust-top lacustrine-lagoonal basin development in accretionary wedges: late Messinian (Lago-Mare) episode in the central Apennines (Italy): *Palaeogeography, Palaeoclimatology, Palaeoecology*, v. 151, p. 149–166, [https://doi.org/10.1016/S0031-0182\(99\)00026-7](https://doi.org/10.1016/S0031-0182(99)00026-7).
- Cipollari, P., Cosentino, D., and Gliozzi, E., 1999b, Extension- and compression-related basins in central Italy during the Messinian Lago-Mare event: *Tectonophysics*, v. 315, p. 163–185, [https://doi.org/10.1016/S0040-1951\(99\)00287-5](https://doi.org/10.1016/S0040-1951(99)00287-5).
- Conti, P., Cornamusi, G., and Carmignani, L., 2020, An outline of the geology of the Northern Apennines (Italy), with geological map scale 1:250,000: *Italian Journal of Geoscience*, v. 139, no. 2, p. 149–194, <https://doi.org/10.3301/IJG.2019.25>.
- Conticelli, S., and Peccherillo, S., 1992, Petrology and geochemistry of potassic and ultrapotassic volcanism in central Italy: Petrogenesis and inferences on the evolution of the mantle sources: *Lithos*, v. 28, p. 221–240, [https://doi.org/10.1016/0024-4937\(92\)90008-M](https://doi.org/10.1016/0024-4937(92)90008-M).
- Corrado, S., 1995, Optical parameters of maturity of organic matter dispersed in sediments: First results from the Central Apennines (Italy): *Terra Nova*, v. 7, p. 338–347, <https://doi.org/10.1111/j.1365-3121.1995.tb00803.x>.
- Corrado, S., Di Bucci, D., Naso, G., Giampaolo, C., and Adatte, T., 1998, Application of organic matter and clay mineral studies to the tectonic history of the Abruzzo-Molise-Sannio area, Central Apennines, Italy: *Tectonophysics*, v. 285, p. 167–181, [https://doi.org/10.1016/S0040-1951\(97\)00195-9](https://doi.org/10.1016/S0040-1951(97)00195-9).
- Corrado, S., Aldega, L., Di Leo, P., Giampaolo, C., Invernizzi, C., Mazzoli, S., and Zattin, M., 2005, Thermal maturity of the axial zone of the southern Apennines fold-and-thrust belt (Italy) from multiple organic and inorganic indicators: *Terra Nova*, v. 17, p. 56–65, <https://doi.org/10.1111/j.1365-3121.2004.00584.x>.
- Cosentino, D., Cipollari, P., Di Donato, V., Sgroso, I., and Sgroso, M., 2002, The Volsci Range in the kinematic evolution of the northern and southern Apennines orogenic system: *Bollettino della Società Geologica Italiana*, volume speciale, v. 1, p. 209–218.
- Cosentino, D., Cipollari, P., and Pipponzi, G., 2003, Il sistema orogenico dell'Appennino centrale: Vincoli stratigrafici e cronologia della migrazione: *Studi Geologici Camerti*, numero speciale, p. 87–101.
- Cosentino, D., Cipollari, P., Lo Mastro, S., and Giampaolo, C., 2005, High-frequency cyclicity in the latest Messinian Adriatic foreland basin: Insight into palaeoclimate and palaeoenvironments of the Mediterranean Lago-Mare episode: *Sedimentary Geology*, v. 178, p. 31–53, <https://doi.org/10.1016/j.sedgeo.2005.03.010>.
- Cosentino, D., Federici, I., Cipollari, P., and Gliozzi, E., 2006, Environments and tectonic instability in central Italy (Gargliano Basin) during the late Messinian Lago-Mare episode: *New data from the onshore Mondragone 1 well: Sedimentary Geology*, v. 188–189, p. 297–317, <https://doi.org/10.1016/j.sedgeo.2006.03.010>.
- Cosentino, D., Miccadei, E., Barberi, R., Basilici, G., Cipollari, P., Parotto, M., and Piacentini, T., 2008, Note Illustrative della carta geologica d'Italia alla scala 1:50,000, foglio 357-Cittaducale: Servizio Geologico d'Italia, 144 p.
- Cosentino, D., Cipollari, P., Di Bella, L., Esposito, A., Faranda, C., Giordano, G., Gliozzi, E., Mattei, M., Maazini, I., Porreca, M., and Funicello, R., 2009, Tectonics, sea-level changes and palaeoenvironments in the early Pleistocene of Rome (Italy): *Quaternary Research*, v. 72, p. 143–155, <https://doi.org/10.1016/j.yqres.2009.03.003>.
- Cosentino, D., Cipollari, P., Marsili, P., and Scrocca, D., 2010, Geology of the central Apennines: A regional review: *Journal of the Virtual Explorer*, v. 36, <https://doi.org/10.3809/jvirtex.2010.00223>.
- Cosentino, D., Asti, R., Nocentini, M., Gliozzi, E., Kotsakis, T., Mattei, M., Esu, D., Spadi, M., Tallini, M., Cifelli, F., Pennacchioni, M., Cavuoto, G., and Di Fiore, V., 2017, New insights into the onset and evolution of the central Apennine extensional intermontane basins based on the tectonically active L'Aquila Basin (central Italy): *Bulletin of the Geological Society of America*, v. 129, p. 1314–1336, <https://doi.org/10.1130/B31679.1>.
- Cosentino, D., Bracone, V., D'Amico, C., Cipollari, P., Esu, D., Faranda, C., Frezza, V., Gliozzi, E., Grossi, F., Guerrieri, P., Iadanza, A., Kotsakis, T., and Soulié-Märsche, I., 2018, The record of the Messinian salinity crisis in mobile belts: Insights from the Molise allochthonous units (southern Apennines, Italy): *Palaeogeography, Palaeoclimatology, Palaeoecology*, v. 503, p. 112–130, <https://doi.org/10.1016/j.palaeo.2018.04.028>.
- Cramer, F., Lithgow-Bertelloni, C.R., and Tackley, P.J., 2017, The dynamical control of subduction parameters on surface topography: *Geochimica et Geophysica*, v. 18, p. 1661–1687, <https://doi.org/10.1002/2017GC006821>.
- D'Agostino, N., Jackson, J.A., Dramis, F., and Funicello, R., 2001, Interactions between mantle upwelling, drainage evolution and active normal faulting: An example from the central Apennines (Italy): *Geophysical Journal International*, v. 147, p. 475–497, <https://doi.org/10.1046/j.1365-246X.2001.00539.x>.
- De Rita, D., Bertagnini, A., Faccenna, C., Landi, P., Rosa, C., Zarlunga, F., Di Filippo, M., and Carboni, M.G., 1997, Evoluzione geotopografica-strutturale dell'area tolfetana: *Bollettino della Società Geologica Italiana*, v. 116, p. 143–175.
- Diaferia, G., Cammarano, F., and Faccenna, C., 2019, Thermal structure of a vanishing subduction system: An example of seismically-derived crustal temperature along the Italian peninsula: *Geophysical Journal International*, v. 219, p. 239–247, <https://doi.org/10.1093/gji/ggz289>.
- Duretz, T., and Gerya, T.V., 2013, Slab detachment during continental collision: Influence of crustal rheology and interaction with lithospheric delamination: *Tectonophysics*, v. 602, p. 124–140, <https://doi.org/10.1016/j.tecto.2012.12.024>.
- Faccenna, C., and Becker, T.W., 2020, Topographic expressions of mantle dynamics in the Mediterranean: *Earth-Science Reviews*, v. 209, no. 103327, <https://doi.org/10.1016/j.earscirev.2020.103327>.
- Faccenna, C., Becker, T.W., Miller, M.S., Serpelloni, E., and Willett, S.D., 2014, Isostasy, dynamic topography, and the elevation of the Apennines of Italy: *Earth and Planetary Science Letters*, v. 407, p. 163–174, <https://doi.org/10.1016/j.epsl.2014.09.027>.
- Faccenna, C., Funicello, R., Bruni, A., Mattei, M., and Sagnotti, L., 1994, Evolution of a transfer-related basin: The Ardea basin (Latium, central Italy): *Basin Research*, v. 6, p. 35–46, <https://doi.org/10.1111/j.1365-2117.1994.tb00073.x>.
- Faure Walker, J.P., Roberts, G.P., Cowie, P.A., Papanikolaou, I., Michetti, A.M., Sammonds, P., Wilkinson, M., McCaffrey, K.J.W., and Phillips, R.J., 2012, Relationship between topography, rates of extension and mantle dynamics in the actively-extending Italian Apennines: *Earth and Planetary Science Letters*, v. 325–326, p. 76–84, <https://doi.org/10.1016/j.epsl.2012.01.028>.
- Fellin, M.G., Reiners, P.W., Brandon, M.T., Wüthrich, E., Balestrieri, E., and Molli, G., 2007, 2077, Thermochronologic evidence for the exhumation history of the Alpi Apuane metamorphic core complex, northern Apennines, Italy: *Tectonics*, v. 26, no. 6, <https://doi.org/10.1029/2006TC002085>.
- Festa, A., Ghisetti, F., and Vezzani, L., 2006, Carta Geologica del Molis: Note Illustrative: Regione Molise—Presidenza della Giunta, Litografia GEDA, Nichelino (TO), Italy, scale 1:100,000.
- Flowers, R.M., Ketcham, R.A., Shuster, D.L., and Farley, K.A., 2009, Apatite (U-Th)/He thermochronometry using a radiation damage accumulation and annealing model: *Geochimica et Cosmochimica Acta*, v. 73, p. 2347–2365, <https://doi.org/10.1016/j.gca.2009.01.015>.
- Fox, M., Dai, J.-G., and Carter, A., 2019, Badly behaved detrital (U-Th)/He ages: Problems with He Diffusion models or geological models?: *Geochimica et Geophysica*, v. 20, p. 2418–2432, <https://doi.org/10.1029/2018GC008102>.

- Fubelli, G., Falcucci, E., Mei, A., and Dramis, F., 2008, Evoluzione quaternaria del bacino di Leonessa (Rieti): Il Quaternario, v. 21, p. 457–468.
- Fubelli, G., Della Seta, M., and Amato, G., 2014, Drainage system adjustment in response to the opening of the Rieti intermontane basin (Central Italy): Geostatistical reconstruction of the Paleofarfa River alluvial plain: Rendiconti Lincei, v. 25, p. 167–176, <https://doi.org/10.1007/s12210-014-0322-0>.
- Gallagher, K., 2012, Transdimensional inverse thermal history modeling for quantitative thermochronology: Journal of Geophysical Research. Solid Earth, v. 117, p. 1–16, <https://doi.org/10.1029/2011JB008825>.
- Gautheron, C., Tassan-Got, L., Barbarand, J., and Pagel, M., 2009, Effect of alpha-damage annealing on apatite (U-Th)/He thermochronology: Chemical Geology, v. 266, p. 157–170, <https://doi.org/10.1016/j.chemgeo.2009.06.001>.
- Giaccio, B., Castorina, F., Nomade, S., Scardia, G., Voltaggio, M., and Sagnotti, L., 2013, Revised chronology of the Sulmona lacustrine succession, central Italy: Journal of Quaternary Science, v. 28, p. 545–551, <https://doi.org/10.1002/jqs.2647>.
- Giaccio, B., Leicher, N., Mannella, G., Monaco, L., Regattieri, E., Wagner, B., Zanchetta, G., Gaeta, M., Marra, F., Nomade, S., Palladino, D.M., Pereira, A., Scheidt, S., Sottili, G., Wonik, T., Wulf, S., Zeeden, C., Ariztegui, D., Cavinato, G.P., Dean, J.R., Florindo, F., Leng, M.J., Macrì, P., Niespolo, E., Renne, P.R., Rolf, C., Sadori, L., Thomas, C., and Tzedakis, P.C., 2019, Extending the tephra and palaeoenvironmental record of the Central Mediterranean back to 430 ka: A new core from Fucino Basin, central Italy: Quaternary Science Reviews, v. 225, no. 106003, <https://doi.org/10.1016/j.quascirev.2019.106003>.
- Göğüş, O.H., Pysklywec, R.N., Şengör, A.M.C., and Gün, E., 2017, Drip tectonics and the enigmatic uplift of the Central Anatolian plateau: Nature Communications, v. 8, no. 1538, <https://doi.org/10.1038/s41467-017-01611-3>.
- Gvirtzman, Z., and Nur, A., 2001, Residual topography, lithospheric structure and sunken slabs in the central Mediterranean: Earth and Planetary Science Letters, v. 187, p. 117–130, [https://doi.org/10.1016/S0012-821X\(01\)00272-2](https://doi.org/10.1016/S0012-821X(01)00272-2).
- Hourigan, J.K., Reiners, P.W., and Brandon, M.T., 2005, U-Th zonation-dependent alpha-ejection in (U-Th)/He chronometry: Geochemistry et Cosmochimica Acta, v. 69, p. 3349–3365, <https://doi.org/10.1016/j.gca.2005.01.024>.
- Hyndman, R.D., and Currie, C.A., 2011, Why is the North America Cordillera high? Hot backarcs, thermal isostasy, and mountain belts: Geology, v. 39, no. 8, p. 783–786, <https://doi.org/10.1130/G31998.1>.
- Malinverno, A., and Ryan, W.B.F., 1986, Extension in the Tyrrhenian sea and shortening in the Apennines as result of arc migration driven by sinking of the lithosphere: Tectonics, v. 5, p. 227–245, <https://doi.org/10.1029/TC005i002p0227>.
- Mancini, M., D'Anastasio, E., Barbieri, M., and De Martini, P.M., 2007, Geomorphological, paleontological and  $^{87}\text{Sr}/^{86}\text{Sr}$  isotope analyses of early Pleistocene paleoshorelines to define the uplift of Central Apennines (Italy): Quaternary Research, v. 67, p. 487–501, <https://doi.org/10.1016/j.yqres.2007.01.005>.
- Mancini, M., Vignaroli, G., Bucci, F., Cardinali, M., Cavinato, G.P., Di Salvo, C., Giallini, S., Moscatelli, M., Polpetta, F., Putigano, M.L., Santangelo, M., and Sirianni, P., 2020, New stratigraphic constraints for the Quaternary source-to-sink history of the Amatrice Basin (central Apennines, Italy): Geological Journal, v. 55, p. 4226–4251, <https://doi.org/10.1002/gj.3672>.
- Mattei, M., Cipollari, P., Cosentino, D., Argentieri, A., Rossetti, F., Speranza, F., and Di Bella, L., 2002, The Miocene tectono-sedimentary evolution of the Southern Tyrrhenian Sea: Stratigraphy, structural and paleomagnetic data from the on-shore Amantea basin (Calabrian arc, Italy): Basin Research, v. 14, p. 147–168, <https://doi.org/10.1046/j.1365-2117.2002.00173.x>.
- Micarelli, A., and Cantalamessa, G., 2009, Note Illustrative della Carta Geologica d'Italia alla scala 1:50,000, foglio 314-Montegiorgio: Servizio Geologico d'Italia, 90 p.
- Milli, S., Cannata, D., Marini, M., and Moscatelli, M., 2013, Facies and geometries of Lower Messinian Laga Basin turbidite deposits (central Apennines, Italy): Journal of Mediterranean Earth Sciences, v. 5, p. 179–196.
- Mondati, G., Spadi, M., Gliozzi, E., Cosentino, D., Cifelli, F., Cavinato, G.P., Tallini, M., and Mattei, M., 2021, The tectono-stratigraphic evolution of the Fucino Basin (central Apennines, Italy): New insights from the geological mapping of its north-eastern margin: Journal of Maps, v. 17, p. 87–100, <https://doi.org/10.1080/17445647.2021.1880981>.
- Montone, P., Mariucci, M.T., Pondrelli, S., and Amato, A., 2004, An improved stress map for Italy and surrounding regions (central Mediterranean): Journal of Geophysical Research, v. 109, B10410, <https://doi.org/10.1029/2003JB002703>.
- Patacca, E., and Scandone, P., 1989, Post-Tortonian mountain building in the Apennines. The role of the passive sinking of a relic lithosphere slab, in Boriani, A., Bonafede, M., Piccardo, G.B., and Vai, G.B., eds., The lithosphere in Italy: Advances in Earth Sciences: Atti dei Convegni Lincei 80, p. 157–176.
- Patacca, E., Sartori, R., and Scandone, P., 1990, Tyrrhenian basin and Apenninic arcs: Kinematic relations since Late Tortonian times: Memorie della Società Geologica Italiana, v. 45, p. 425–451, [https://doi.org/10.1007/978-94-011-2016-6\\_7](https://doi.org/10.1007/978-94-011-2016-6_7).
- Patacca, E., Scandone, P., Bellatalla, M., Perilli, N., and Santini, U., 1992, La zona di giunzione tra l'arco appenninico settentrionale e l'arco appenninico meridionale nell'Abruzzo e nel Molise: Studi Geologici Camerti, volume speciale, v. 1991, no. 2, p. 417–441.
- Patacca, E., Scandone, P., Di Luzio, E., Cavinato, G.P., and Parotto, M., 2008, Structural architecture of the central Apennines: Interpretation of the CROP 11 seismic profile from the Adriatic coast to the orographic divide: Tectonics, v. 27, no. 3, <https://doi.org/10.1029/2005TC001917>.
- Picotti, V., and Pazzaglia, F., 2008, A new active tectonic model for the construction of the Northern Apennines mountain front near Bologna (Italy): Journal of Geophysical Research, v. 113, p. B08412, <https://doi.org/10.1029/2007JB005307>.
- Piomallo, C., and Morelli, A., 2003, P wave tomography of the mantle under the Alpine-Mediterranean area: Journal of Geophysical Research. Solid Earth, v. 108, no. B2, <https://doi.org/10.1029/2002JB001757>.
- Pizzi, A., 2003, Plio-Quaternary uplift rates in the outer zone of the central Apennines fold-and-thrust belt, Italy: Quaternary International, v. 101–102, p. 229–237, [https://doi.org/10.1016/S1040-6182\(02\)00105-2](https://doi.org/10.1016/S1040-6182(02)00105-2).
- Pondrelli, S., Salimbeni, S., Ekström, G., Morelli, A., Gasperini, P., and Vannucci, G., 2006, The Italian CMT dataset from 1977 to the present: Physics of the Earth and Planetary Interiors, v. 159, p. 286–303, <https://doi.org/10.1016/j.pepi.2006.07.008>.
- Porreca, M., Minelli, G., Ercoli, M., Brobia, A., Mancinelli, P., Cruciani, F., Giorgetti, C., Carboni, F., Mirabella, F., Cavinato, G.P., Cannata, A., Pauselli, C., and Barchi, M.R., 2018, Seismic reflection profiles and subsurface geology of the area interested by the 2016–2017 earthquake sequence (Central Italy): Tectonics, v. 37, p. 1116–1137, <https://doi.org/10.1002/2017TC004915>.
- Reiners, P.W., and Brandon, M.T., 2006, Using thermochronology to understand orogenic erosion: Annual Review of Earth and Planetary Sciences, v. 34, p. 419–466, <https://doi.org/10.1146/annurev.earth.34.031405.125202>.
- Royden, L.H., 1993, The tectonic expression of slab pull at continental convergent boundaries: Tectonics, v. 12, p. 303–325, <https://doi.org/10.1029/92TC02248>.
- Royden, L., and Faccenna, C., 2018, Subduction orogeny and the late Cenozoic evolution of the Mediterranean arcs: Annual Review of Earth and Planetary Sciences, v. 46, p. 261–289, <https://doi.org/10.1146/annurev-earth-060115-012419>.
- Royden, L.H., Patacca, E., and Scandone, P., 1987, Segmentation and configuration of subducted lithosphere in Italy: An important control on thrust-belt and foredeep-basin evolution: Geology, v. 15, p. 714–717, [https://doi.org/10.1130/0091-7613\(1987\)15<714:SACOSL>2.0.CO;2](https://doi.org/10.1130/0091-7613(1987)15<714:SACOSL>2.0.CO;2).
- Rusciadelli, G., Viandante, M.G., Calamita, F., and Cook, A.C., 2005, Burial-exhumation history of the central Apennines (Italy), from the foreland to the chain building: Thermochronological and geological data: Terra Nova, v. 17, p. 560–572, <https://doi.org/10.1111/j.1365-3121.2005.00649.x>.
- San Jose, M., Caves Rugenstein, J., Cosentino, D., Faccenna, C., Fellin, M.G., Ghinassi, M., and Martini, I., 2020, Stable isotope evidence for rapid uplift of the central Apennines since the late Pliocene: Earth and Planetary Science Letters, v. 544, no. 116376, <https://doi.org/10.1016/j.epsl.2020.116376>.
- Spiegel, K., Kohn, B., Belton, D., Berner, Z., and Gleadow, A., 2009, Apatite (U-Th-Sm)/He thermochronology of rapidly cooled samples: The effect of He implantation: Earth and Planetary Science, v. 285, p. 105–114, <https://doi.org/10.1016/j.epsl.2009.05.045>.
- Stalder, N.F., Fellin, M.G., Caracciolo, L., Guillon, M., Winkler, W., Milli, S., Moscatelli, M., and Critelli, S., 2018, Dispersal pathways in the early Messinian Adriatic foreland and provenance of the Laga Formation (Central Apennines, Italy): Sedimentary Geology, v. 375, p. 289–308, <https://doi.org/10.1016/j.sedgeo.2017.09.016>.
- Thomson, S.N., Brandon, M.T., Reiners, P.W., Zattin, M., Isaacson, P.J., and Balestrieri, M.L., 2010, Thermochronologic evidence for orogen-parallel variability in wedge kinematics during extending convergent orogenesis of the northern Apennines, Italy: Geological Society of America Bulletin, v. 122, p. 1160–1179, <https://doi.org/10.1130/B26573.1>.
- Vezzani, L., Festa, A., and Ghisetti, G.C., 2010, Geology and tectonic evolution of the central-southern Apennines, Italy: Geological Society of America Special Paper, v. 469, 58 p., <https://doi.org/10.1130/2010.2469>.
- Wortel, M.J.R., and Spakman, W., 2000, Subduction and slab detachment in the Mediterranean–Carpathian region: Science, v. 290, p. 1910–1917, <https://doi.org/10.1126/science.290.5498.1910>.
- Zattin, M., Picotti, V., and Zuffa, G.G., 2002, Fission-track reconstruction of the front of the Northern Apennine thrust wedge and overlying Ligurian unit: American Journal of Science, v. 302, p. 346–379, <https://doi.org/10.2475/aj.s.302.4.346>.
- Zhong, S., and Gurnis, M., 1994, Controls on trench topography from dynamic models of subducted slabs: Journal of Geophysical Research. Solid Earth, v. 99, p. 15683–15695, <https://doi.org/10.1029/94JB00809>.

SCIENCE EDITOR: BRAD S. SINGER  
ASSOCIATE EDITOR: WILLIAM GUENTHER

MANUSCRIPT RECEIVED 14 MARCH 2021  
REVISED MANUSCRIPT RECEIVED 9 AUGUST 2021  
MANUSCRIPT ACCEPTED 28 SEPTEMBER 2021

Printed in the USA